27/02/2006

CRISTINA SABATER ANGLADA
Universitat de Girona

Final degree project

FRICTION STIR PROCESSING, a new microstructure improvement technique.

Advisor: Bertrand Huneau
Ecole Centrale de Nantes

1. INTRODUCTION

In 1991 friction stir welding (FSW) was invented at the 'The Welding Institute' (TWI) of United Kingdom [1,2,5]. Throughout the last decade, it has been used as a solid state welding technique, especially for aluminium alloys.

On the bases of FSW, Friction Stir Processing (FSP) [2] has emerged as a microstructure improvement technique. FSP leads to uniform microstructures consisting of very fine grains and high grain boundary misorientations, microstructural features that are considered important for enhanced mechanical properties.

Transportation industry uses a wide range of aluminium alloys. Cast aluminium alloys are wide used for suspension and drive line components in automobiles. FSP can be used to modify microstructures to improve the surface properties of metals, a capability that is of particular interest for transportation applications. Aluminium alloys with high design flexibility are also desired. FSP can easily induce a fine equiaxed microstructure of the same magnitude experienced in many severe plastic deformation techniques such as equal channel angular pressing with a single rastering pass.

In the present work, microstructure improvement using FSP is studied.

The previous will be the bibliographic study of the process, the next the experimental work. It will be divided in three parts:

In the first part of the work, the microstructure improvement of as-cast A356 is demonstrated. Some tensile tests were applied to check the increase in ductility. However, the expected results couldn't be achieved.

In the second part, the microstructure improvement of a fusion weld in 1050 aluminium alloy is presented. Hardness tests were carried out to prove the mechanical property improvements.

In the third and last part, the microstructure improvement of 1050 aluminium alloy is achieved. A discussion of the mechanical property improvements induced by FSP is made. The influence of tool traverse speed on microstructure and mechanical properties is also discussed. Hardness tests and recrystallization theory enabled us to find out such influence.

2. FRICTION STIR WELDING

FSW was invented at The Welding Institute (TWI) of UK in 1991 as a solid state joining technique [1,2,5]. The basic concept is: a non consumable rotating tool with a specially designed pin and shoulder is inserted into the edges of the plates to be joined and traversed along the line of joint (Figure 1).

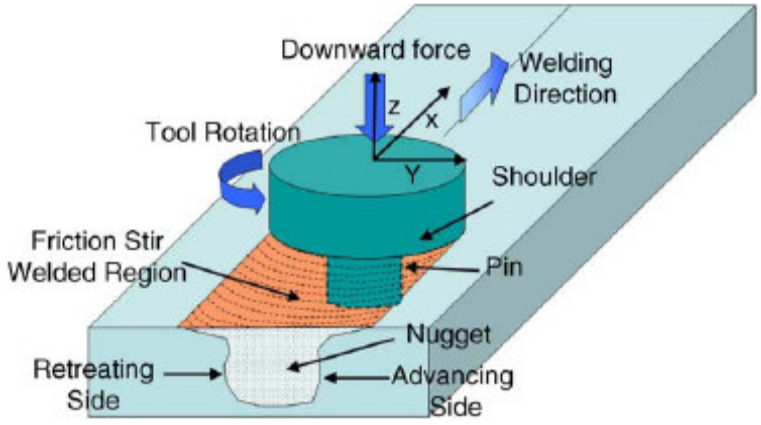

Figure 1. Schematic drawing of friction stir welding [2].

The tool serves two primary functions: heating of workpiece and movement of material to produce the joint. The heating is accomplished by friction between the tool and the workpiece and the plastic deformation of workpiece. The localized heating softens the material around the pin and combination of tool rotation and translation leads to movement of material from the front of the pin to the back of the pin. Thus, the material undergoes intense plastic deformation at elevated temperature. As a result of this process a joint with fine and equiaxed recrystallized grains is produced in solid state. This fine microstructure produces good mechanical properties.

As compared to the conventional welding methods, the key benefits of FSW are summarized in table 1.

Metallurgical benefits	Enviromental benefits	Energy benefits
Solid phase process Low distortion of workpiece Good dimensional stability and repeatability No loss of alloying elements Excellent metallurgical Properties in the joint Fine microstructure Absence of cracking Replace multiple parts joined by fasteners	No shielding gas required No surface cleaning required Eliminate grinding wastes Eliminate solvents required for degreasing Consumable materials saving, such as rugs, wire or any other gases	Improve materials use (e.g. joining different thickness allows reduction in weight) Only 2,5% of the energy needed for a laser weld Decreased fuel consumption in light weight

Table 1. Key benefits of FSW [2].

3. FRICTION STIR PROCESSING

3.1 The process

Friction Stir Processing (FSP) [2-4] is an emerging surface-engineering technology based on friction stir welding (FSW)[1,2,5]. However, the same methodology as FSW is used FSP modifies the local microstructure and does not join metals together.

A schematic illustration of FSP is shown in Figure 1.

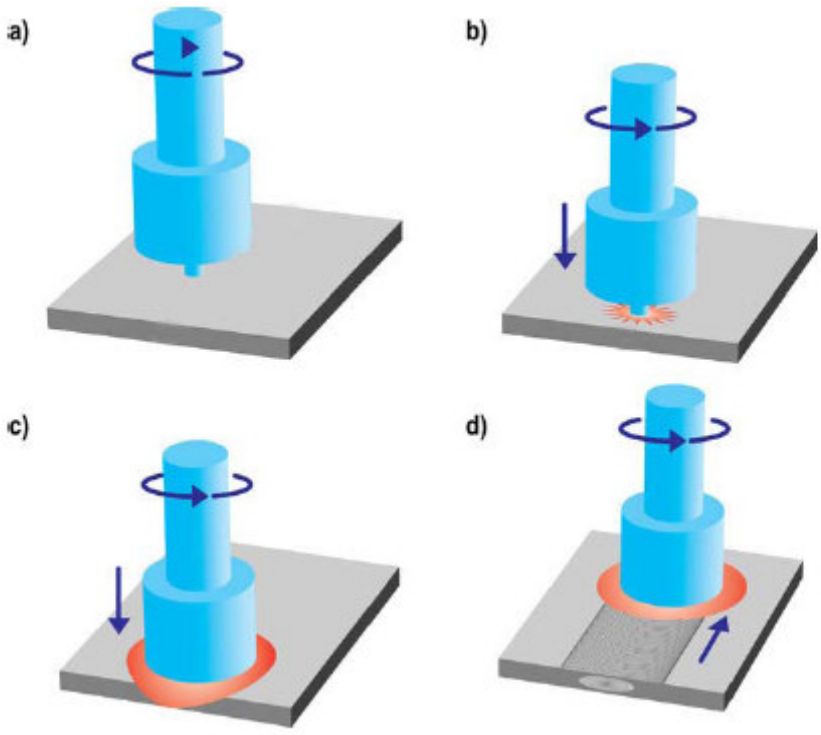

Figure 1. Schematic illustration of friction stir processing: a) rotating tool prior to contact with the plate; b) tool pin makes contact with the plate, creating heat; c) shoulder makes contact, restricting further penetration while expanding the hot zone; and d) plate moves relative to the rotating tool, creating a fully recystallized, fine grain microstructure [3].

To friction process a location within a plate or sheet, a specially designed cylindrical tool is rotated and plunged into the selected area. The tool has a small diameter pin with a concentric larger diameter shoulder. Figure 2 shows a typical tool used in friction stir processing.

Figure 2. Typical FSP tool [4].

When descended to the part, the rotating pin contacts the surface and rapidly friction heats and softens a small column of metal. The tool shoulder and length of entry pin control the penetration depth.
When the shoulder contacts the metal surface, its rotation creates additional frictional heat and plasticizes a larger cylindrical metal column around the inserted pin. The shoulder provides a forging force that contains the upward metal flow caused by the tool pin.
During FSP, the area to be processed and the tool are moved relatively to each other such that the tool traverses until the entire selected area is processed to a fine grain size. The rotating tool provides a continual hot working action, plasticizing metal within a narrow zone, while transportating metal from the leading face of the pin to its trailing edge. The processed zone cools, without solidification, as there is no liquid, forming a defect-free recystallized, fine grain microstructure. Also a closure of porosity and redistribution of inclusions is obtained.

The machine used in FSP is the same used in FSW. Similar to a milling cutter, assures the tool translation and rotation movement. Moreover, provides the suitable support for the plate to be processed. Figure 3 shows a typical friction stir processing machine.

Figure 3. FSW/FSP machine [5].

3.2 Applications

FSP produce improvements in a variety of properties. FSP results in an improvement of strength and ductility, increase resistance to corrosion and fatigue, enhance formability, and improve other properties. Some examples include conditioning microstructures of Al alloys for high strain rate superplastic deformations, incorporating ceramic particle into surface layers of aluminium alloys to form surface composites and improving the mechanical properties of both Al castings and fusion welds of Al plates.

- Microstructure conditioning of Al alloys for high strain rate superplastic deformations.

FSP is a new thermo-mechanical processing technique that leads to a microstructure amenable for high strain rate superplasticity in commercial aluminium alloys.
It is well known that two basic requirements are necessary for achieving structural superplasticity. The first is a fine grain size, typically less than 15 μm. The second is thermal stability of the fine microstructure at high temperatures.
FSP, compared to conventional thermo-mechanical processing (TMP), produces combination of both very fine grain size with high grain boundary misorientation angles and thermal stability.

It has been demonstrated that grains found in friction stir processed aluminium 7050 alloy arise as a result of nucleation and growth within a heavily deformed structure and not from the rotation of pre-existing subgrains [6].

Moreover, it has been pointed out that the optimum strain rate for maximum elongation at 490° C is 1 x 10e-2 s-1 in 7075 Al alloy with an activation energy of 239 Kj mol-1, close to that of grain boundary diffusion [7].

Recently, superplasticity in as cast A365 has been induced via friction stir welding. The microstructure of the cast alloy consists of primary Al alloy dendrites with interdendritic regions of Al intermetallic phases and elemental Si. By comparison, in the FSP a fine and equiaxed Si particles are uniformly distributed in the aluminium matrix due to an intense breakup of the as-cast microstructure and sequent material mixing. The optimum strain rate for maximum elongation at 530ºC is 1 x 10e-2 s-1. Such largest superplasticity is attributed to the fine-grained microstructure achieved via FSP. Not always the superplasticity is associated only with a fine-grained microstructure but also with the appearance of a liquid phase as in metal matrix composites [8].

The overall demonstrates that FSP is a very effective processing technique to create a thermally stable fine-grained microstructure in cast aluminium alloys resulting in a significant superplasticity.

- Ceramic particle incorporation into surface layers of aluminium alloys to form surface composites.

Compared to unreinforced metals, metal matrix composites reinforced with ceramic phases exhibit high strength, high elastic modulus, improved resistance to wear, creep and fatigue, which make them promising structural materials for aerospace and automobile industries. However, these composites also suffer from a great loss in ductility and toughness due to incorporation of non-deformable ceramic reinforcements, which limits their applications to a certain extent.
For many applications, the useful life component often depends on their surface properties such as wear resistance. In these situations, it is desiderable that only the surface layer of components is reinforced by ceramic phases while the bulk of components retain the original composition and structure with higher toughness.

FSP is a very effective technique to fabricate surface metal matrix composite with well-distributed particles and very good bonding with metal substrate.
The advantages of FSP are evident compared with the conventional methods such as laser processing, high-energy beam irradiation and casting sinter.
Firstly, the FSP is carried out in solid state, so interfacial reaction and formation of detrimental phases are avoided. Therefore, it is suitable for processing various kinds of aluminium alloys and other metals.
Secondly, the FSP results in a significant grain refinement in surface layer. The wrought microstructure is desiderable for enhanced the fracture properties as compared with the solidified microstructure that results from laser processing or high-energy electron beam irradiation.
Thirdly, FSP operation is relatively simple and easy controlled because no complicated device is needed.
In recent studies, surface layers of 50-200 μm with well-distributed particles and very good bonding with aluminium substrated have been generated. The microhadness of the surface composite was doubled [9].

- Mechanical properties of Al castings.

Some Al alloys such as A365, A319 and Nickel Aluminium Bronze are widely used to cast high-strength with good casting characteristics. However, some mechanical properties of cast alloys, in particular ductility, toughness and fatigue resistance, are limited by porosity, coarse particles and coarse dendrites.
FSP results in an improvement in several mechanical properties such as strength, ductility, toughness, fatigue, and corrosion resistance.

For A365 and A319 alloys, the cast structure consist of a primary Al alloy dendrites with interdendritic regions of Al intermetallic phases and elemental Si. Both also contain relatively large primary intermetallic particles and shrinkage porosity.

The stirring action of FSP on these microstructures closed porosity, fractured large second-phase particles reducing both their average size and ratios and uniformly distributed particles throughout the stir zone microstructure. Traces of dendritic solidification were eliminated throughout the stir zones.
Soft spots found in the casting due to porosity and Al dendrite cores were eliminated by FSP increasing their hardness.
As porosity levels and microstructure scale decreased (Hall-Petch relationship) ductility and tensile strength increased. Generally, the improved ductility is accompanied by an increase of yield strength and ultimate tensile strength as well.
The fatigue properties of Al castings depend on not only the porosity and second-phase particles, but on their sizes, shapes and distributions in microstructures. The FSP reduce porosity and more uniformly sized and distributed second-phase particles of aspect ratio. These types of microstructure modifications imply better fatigue properties.

The significant improvement in mechanical properties of FSP is attributed to microstructural refinement (both aluminium matrix and Si particles) and homogenization and elimination of porosity [10,11].

Many cast components produced in NAB involve thick sections and the slow cooling rates contribute to coarse microstructures and reduced mechanical properties.
FSP convert as-cast microstructure to a wrought condition creating a variety of microstructures. These microstructures include lamellar, fine grain and Widmanstätten. Either a composite of microstructures can be created by FSP. All FSP microstructures have significantly superior mechanical properties compared to the as-cast microstructure. This is due to the large deformations in the softened regions, and so microstructure refinement and homogenization improved strength and ductility. FSP may also result in a closure of porosity and redistribution of inclusions thus conferring improved corrosion and fatigue resistance. The greatest property increase was achieved when microstructural morphology was entirely Widmänstatten (no macro orientation bias observed), yield strength increase 170% and tensile strength 85%. Also ductility is better than for the cast alloy [12,13].

- Mechanical properties improvement fusion welds of Al plates.

It will not be possible to friction stir weld all aluminium structures and reap the benefits of this solid state process. For example, large structures, inaccessible locations, and very thick plate would be difficult to friction stir weld. However, eventually it may be possible to friction stir process the surface of fusion welds. By friction stir processing the surface, the cast fusion weld microstructure will be converted to a fully recrystallized fine grain and weld defects near the surface will be eliminated. Potential benefits include both increased corrosion resistance and fatigue life.

Automated metal inert gas (MIG) welding of 6mm thick 5083-H321 Al was performed parallel to the longitudinal direction of rolled plates using a 5356 Al weld filler alloy. FSP was applied. The fusion weld region with a coarse-grain microstructure and porosity compared to that of a cast alloy turn into a fine equiaxed grains microstructure as a result of mixing both the fusion weld and the parent metal alloy [3].

Laser Beam Welding (LBW) and FSP processes have been applied to the equal channel angular pressed (ECA) aluminium alloy 1050 with the thickness of 1mm [14].The ECA pressed alloy after two passes through the die consisted of a cell structure with cell size of about 0.58 μm and the hardness value was approximately 46 Hv. The LBW produced as-cast coarse microstructure and coarse equiaxed grain structure at the fusion zone and the HAZ respectively, which led to a hardness reduction to <30 Hv in the LB weld. On the other hand, fine homogenised microstructure was obtained by FSP the weld, introducing its particular heat generation and plastic strain. Thus, led to a high hardness due to the decrease of the grain size (Hall-Petch relationship) [15].

4. PROCESS PARAMETERS

FSP involves complex material movement and plastic deformation. Tool geometry and processing parameters such as tool traverse speed, tool rotation rate, target depth and preheating or cooling, exert significant effect on the material flow pattern and the temperature distribution, thereby influencing the microstructural evolution of material.

4.1 Tool geometry

The tool geometry plays a critical role in material flow. Considering such significant effect of tool geometry on the metal flow, fundamental correlation between material flow and resultant microstructure of the processed zones varies with each tool.

A FSP tool consists of a shoulder and a pin as shown in figure 1.

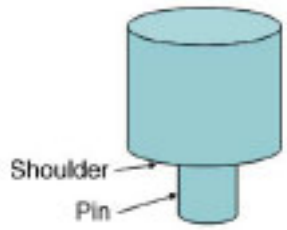

Figure 1. Schematic drawing of the FSP tool [2].

As mentioned earlier, the tool has two primary functions: localized heating and material flow.

The first function of the tool is generating heat during the process. In the initial stage of the plunge, the heating results primarily from the friction between pin and workpiece. Some additional heating, results from deformation of material. The tool is plunged till the shoulder touches the workpiece. The friction between the shoulder and workpiece results in the biggest component of heating. Form the heating aspect, the relative size of the shoulder is important, and the other design features are not critical. The shoulder also provides confinement for the heated volume of material. Generally concave shoulders are used.

The second function of the tool is to stir and move the material. This is the pin's primary function. A well-designed pin enable easier flow of plasticized material, increase the ratio of swept volume during rotation to the volume of the pin itself, improving the flow path around and underneath the pin and increase the interface between the pin and the plasticized material, increasing heat generation. Moreover, suitable pin geometry reduces process loads. Generally cylindrical pins are used.

After all, it is important to realise that generalization of microstructural development and influence of processing parameters is difficult in absence of the tool information.

For the first part of the present study a tool with a con-shaped pin was used. Diameter shoulder was 20 mm, bigger diameter pin was 6 mm, smaller diameter pin was 3 mm and pin length was 4 mm. Figure 2 shows the used tool.

Figure 2. Tool used in microstructural refinement of A356.

For the second and third part, two tools were machined. One without pin and the other with a 1 mm high and 10 mm diameter cylindrical pin, both with a flat shoulder of 20 mm diameter. The figure 3 bellow shows the shape of both.

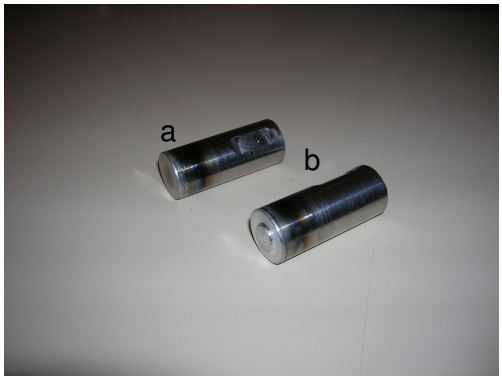

Figure 3. Tools machined for microstructural refinement of the fusion weld and the Al 1050-0 alloy a) was not used, b) was used.

Although in the beginning both were assumed to be suitable for the process. Primary experiments, showed the usefulness of the tool without pin. At the end of the process the heat was so high that even the material was totally melt. Figure 4 shows the result.

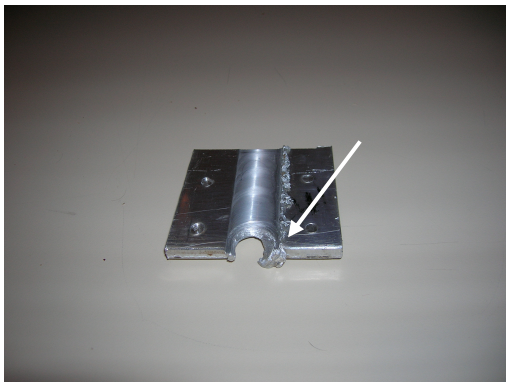

Figure 4. Plate processed with the tool without pin. Metal was melt at the end of the process.

4.2 Processing Parameters

For FSP, two parameters are very important: tool rotation rate (w, rpm) in clockwise or counterclockwise direction and tool traverse speed (v, mm/min) along the processed zone. In addition, the insertion depth of pin into the workpieces, called target depth is an important process parameter.

4.2.1 Tool rotation rate and tool traverse speed

The rotation of the tool results in stirring and mixing of material around the rotating pin. Temperature is observed to be a strong function of the rotation rate. Higher tool rotation rates generate higher temperature because of higher friction heating and result in more intense stirring and mixing of material. However, it should be noted that frictional coupling of tool surface with workpiece is going to govern the heating. So a monotonic increase in heating with increasing tool rotation rate is not expected as the coefficient of friction at interface will change with increasing tool rotation rate. The tool rotation rate ranges from 500 to 1000 rpm.

The translation of the tool moves the stirred material from the front to the back of the pin and finishes the processed zone. Rate of heating is observed to be a strong function of the traverse speed. Higher traverse speeds leads to lower heat generation and higher degree of deformation. The tool traverse speed ranges from 60 mm/min to 360 mm/min.

As discussed before, due to tool rotation rate and traverse speed, FSP involve intense plastic deformation, mixing, and thermal exposure, resulting in significant microstructural changes, a processed zone characterized by recrystallized fine grains and uniformly distributed particles. As these two parameters are so important, it will be helpful to define a ratio tool rotation speed/tool traverse speed, v/w (min^{-1}). In order to study the influence of v and w as processing parameters on the microstructural modifications obtained by FSP, we could modify whether v, whether w or v/w, keeping constant the parameters which were not modified.

In the first part of the present work the FSP was performed at a tool traverse speed of 1 mm/s and a tool rotation rate of 900 rpm.

I the second part, the processing was carried out at a tool traverse speed of 1mm/s and a tool rotation rate of 500 rpm.

In the third part, the choice of tool rotation rate and traverse speed was obtained by comparison with recent studies [15,16,17,18].

Sato et al [15], studied the effect of grain size on hardness in the stir zones of ultra-fined grained specimens of 1050 Al alloy by Hall-Petch relationship. FSP was performed at a tool rotation speed of 800 rpm and 354 m/min. The microstructure and mechanical properties obtained are in Table 1.

w (rpm)	v (mm/min)	w/v (mm^{-1})	Grain size (µm)	Hardness (Hv)
800	354	2,25988701	1	45

Table 1. Processing parameter influence on mechanical properties of Al 1050-0 [15].

Kwon et al [16], produced ultra-fined grained specimens of 1050 Al alloy by FSP and also studied the influence of the tool rotation rate on the microstructure and mechanical properties. FSP was performed with only a single pass at a constant tool traverse speed of 155 m/min and at tool rotation speeds ranging from 560 to 1840 rpm. The following results were found (Table 2):

w (rpm)	v (mm/min)	w/v (mm^{-1})	Grain size (μm)	Hardness (Hv)
560	155	3,61290323	0,5	47,5
980	155	6,32258065	1-2	45
1350	155	8,70967742	2	40
1840	155	11,8709677	3-4	30

Table 2. Processing parameter influence on mechanical properties of Al 1050-0 [16].

From the results above, it was noted that the recrystallized grain size can be reduced by decreasing the tool rotation rate at a constant traverse speed or decreasing the tool rotation rate/traverse speed. FSP at higher tool rotation rate or higher ratio of tool rotation rate/traverse speed results in an increase in both degree of deformation and peak temperature of thermal cycle. The increase in the degree of deformation during FSP results in a reduction in the recrystallized grain size according to the general principles for recrystallization. On the other hand, the increase in peak temperature of FSP thermal cycle leads to generation of coarse recrystallized grains, and also results in a remarkable grain growth. This shows that there is an optimum combination of tool rotation rate and traverse speed for generating the finest grain size in a specific alloy.

As mentioned before lower w/v ratios lead to a better microstructural evolution and mechanical properties for the friction stir processed zones. Lower v/w ratios require low w and high v. Otherwise, we can not decrease w below a certain limit. Also, increase v above a certain limit is not possible. In this study we will try to find out the optimum ratio in order to achieve the needed stirring and mixing action that produces the right adiabatic heating and local softening to achieve the best microstructure and mechanical properties.

FSP will be carried out at constant tool rotation rate of 500 rpm and tool traverse speeds ranging from 60 mm/min to 360 mm/min. Known et al, in their studies [16] they did the contrary. They maintained constant the tool rotation rate and varied the tool traverse speed.
The processing parameters are collected in the Table 3:

	w (rpm)	v (mm/min)	w/v (mm^{-1})
MICROSTRUCTURAL REFINEMENT OF A356	900	60	15
MICROSTRUCTURAL REFINEMENT OF A FUSION WELD IN Al 1050-O	500	60	8,33333333
MICROSTRUCTURAL REFINEMENT OF Al 1050-O	500	60	8,33333333
	500	120	4,16666667
	500	180	2,77777778
	500	240	2,08333333
	500	300	1,66666667
	500	360	1,38888889

Table 3. Processing parameters used in the present work.

4.2.2 Target depth

The insertion depth of pin into the workpiece is important for producing sound processing zones with smooth tool shoulders. The insertion depth of pin is associated with the pin height.

When the insertion depth is too shallow, the shoulder of tool does not contact the original workpiece surface. Thus rotating shoulder cannot move the stirred material efficiently from the front to the back of the pin, resulting in generation of processed zones with inner channel or surface groove. During the experimental work, we faced this problem. Figure 5 shows a processed plate with surface groove.

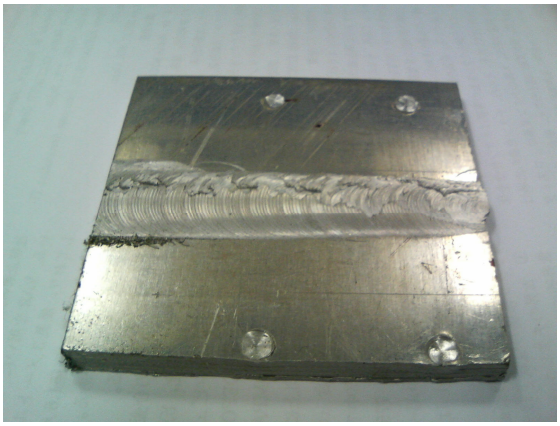

Figure 5. Processed plate with surface groove.

When the insertion depth is too deep, the shoulder of tool plunges into the workpiece creating excessive flash. In this case, a significantly concave processed zone is produced, leading to local thinning of the processed plates. Figure 6 shows a plate with such problem.

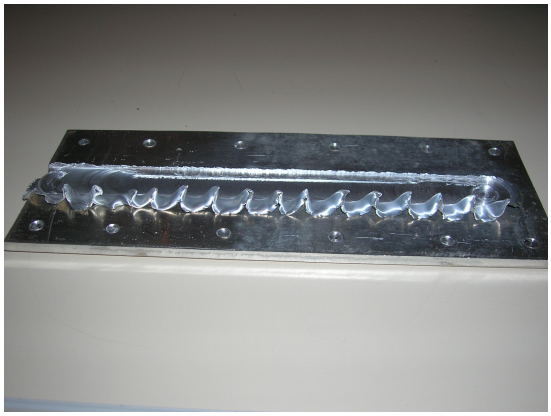

Figure 6. Processed plate with excessive flash.

4.2.3 Preheating or cooling

Preheating or cooling can also be important for some specific FSP processes. For materials with high melting point such as steel and titanium or high conductivity such as copper, the heat produced by friction and stirring may be not sufficient to soften and plasticize the material around the rotating tool. Thus it is difficult to produce defect free processed zones. In these cases, preheating or additional external heating source can help the material flow. On the other hand, materials with lower melting point such as

aluminium, cooling can be used to reduce extensive growth of recrystallized grains in and around the processed zone.

In the present work, although the processed material was aluminium, a preheating of 20 seconds in the beginning was performed with no additional cooling.

5. THE PROFILE OF THE PROCESSED ZONE

From the macrostructural point of view the processed zone presents three main characteristics (Figure 1):

-The first one is the presence of a keyhole. At the end of the process, when the tool is pulled out of the workpiece, it leaves behind an exit hole as a footprint.
-The second is the presence of semicircular footprints (racks) at the top surface of the workpiece due to the tool shoulder.
-The third is the presence of a flash. When the insertion depth is too deep, the shoulder of tool plunges into the workpiece creating a waste of material in a line shape on one of the two processed zone sides.
It is worth to point out that two processed zone sides can be distinguished. One is the advancing side where the tool traverse speed and the tool rotation rate are in the same direction. On the contrary in the retreating side the tool traverse speed and the rotation rate are in the opposite direction. Normally the flash is found on the retreating side.

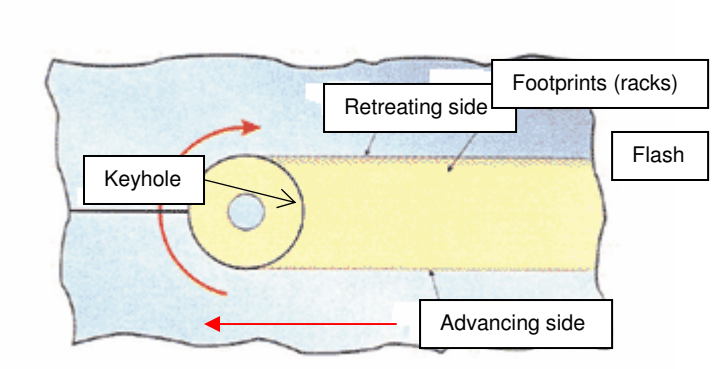

Figure 1. Schema of the processed zone macrostructure.

The contribution of intense plastic deformation and high-temperature exposure within the stirred zone during FSP results in recristallization and development of texture within the stirred zone and precipitate dissolution and coarsening within and arround the stirred zone.

Based on microstructural characterization of grains and precipitates, three distinct zones, stirred zone (nugget), thermo-mechanically affected zone (TMAZ), and heat affected zone (HAZ), have been identified as shown in Figure 2.

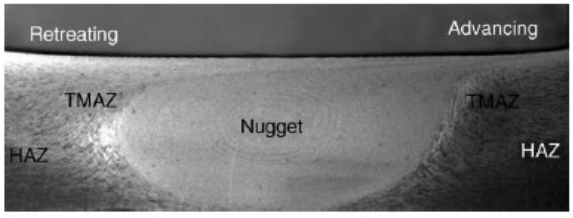

Figure 2. Typical macrograph showing various microstructural zones in FSP 7075Al-T651 [2].

5.1 Nugget

It is the central area of processed zone. Depending on processing parameter, tool geometry, temperature of workpiece, and thermal conductivity of the material, various shape of the nugget have been observed (Figure 3).

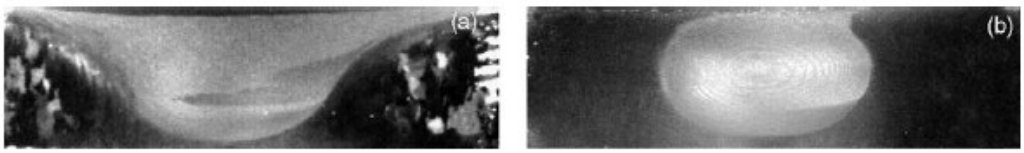

Figure 3. Effect of processing parameter on nugget shape in FSP A356 [2].

This region is usually referred to as dynamically recrystallized zone (DXZ). Intense plastic deformation and frictional heating during FSP result in generation of a recrystallized fine-grained microstructure within the stirred zone. The small recrystallized grains within DXZ have different densities of dislocations and show various degrees of recovery. Moreover, the grain size within the processed zone presents a variation in grain size from the bottom to the top as well as from the advancing to the retreating side. The average grain size at the bottom and retreating side is smaller than the average grain size at the top and advancing side. Such variation is believed to be associated with difference in temperature profile, heat dissipation and degree of deformation in the nugget zone. Figure 4 shows the grain size distribution in various locations of the nugget.

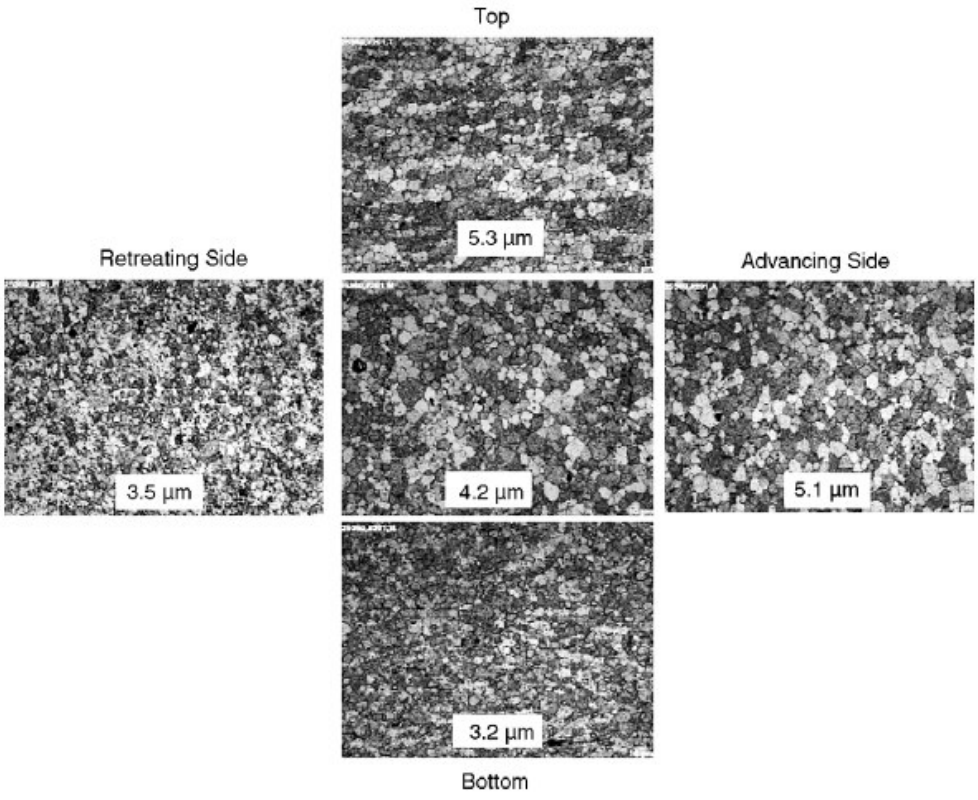

Figure 4. grain size distribution in various locations of 7050Al weld nugget [2].

5.2 Thermomechanically affected zone (TMAZ)

It is a transition zone, thermo-mechanical affected, between the heated affected zone and the nugget zone. The TMAZ experiences both temperature and deformation during FSP. The TMAZ, is mainly characterized by a highly deformed structure, however, some recrystallizated grains are present. The highly deformed structure results from the parent metal deformation grains. The recrystallized grains are similar to the recrystallized grains present in the nugget zone. Figure 5 presents a TMAZ microstructure.

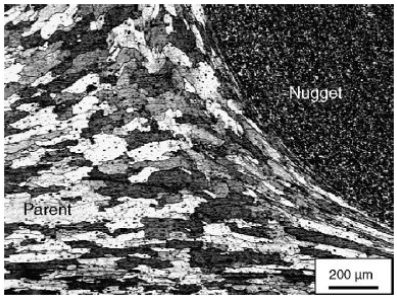

Figure 5. Microstructure of TMAZ in FSP 7075Al [2].

Moreover, the morphology of that zone is different from side to side of the nugget zone. On the retreating side of the tool the interface is relatively diffuse, but quite sharp on the advancing side of the tool. Figure 6 shows such difference.

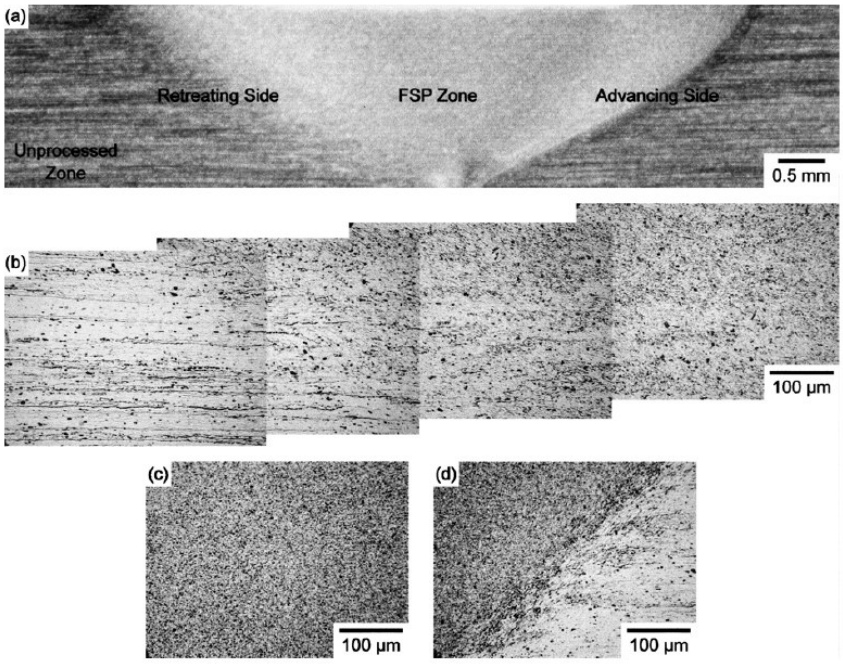

Figure 6 Light microstructures of a cross-section perpendicular to the tool traverse direction in 1050-O; a) overall morphology of the FSP zone, b) transition zone on the retreating side, c) central region and d) transition zone on the advancing side [16].

5.3 Heated affected zone (HAZ)

Beyond the TMAZ there is a heat affected zone. This zone experiences thermal cycle but does not undergo any plastic deformation. The HAZ retains the same grain structure as the parent material. However the thermal exposure exerts a significant effect on the precipitate structure. Figure 7 presents precipitate microstructures in various locations.

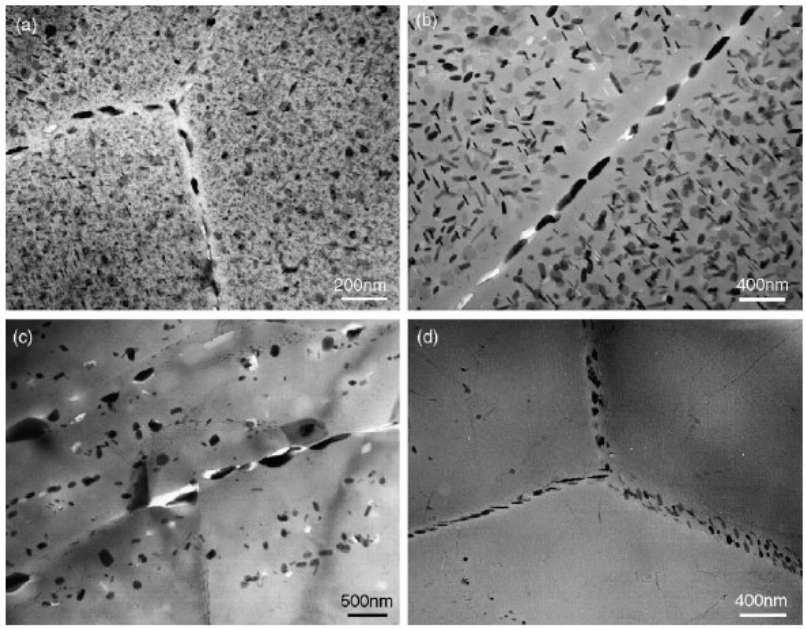

Figure 7. Precipitate microstructures in the grain interior and along grain boundaries in FSW 7050-T651; a) base metal, b) HAZ, c) TMAZ near HAZ, and d) TMAZ near nugget zone [2].

6. TEMPERATURE DISTRIBUTION AND HEAT GENERATION

6.1 Temperature distribution

FSP results in intense plastic deformation around rotating tool and friction between tool and workpieces. Both these factors contribute to the temperature increase within and around the stirred zone. Since the temperature distribution within and around the stirred zone directly influences the microstructure of the processed zone, such as grain size, grain boundary character, coarsening, and resultant mechanical properties, it is important to obtain information about temperature distribution during FSP.
Assuming the heat generation in FSP as a punctual heat source Q_t moving at tool traverse speed V_a, the problem can be solved by Rosenthal equation [19].

$$T_M - T_o = \frac{Q_t}{2\pi\kappa}\exp(\frac{-V_a R}{2a})\exp(\frac{-V_a R}{2a})\frac{1}{R}$$

where,

T_M: temperature at point M (°C)
T_o: initial temperature(°C)
a = $\frac{\kappa}{\rho c}$: thermal diffusivity($\frac{m^2}{s}$)

κ : thermal conductivity($\frac{W}{m°C}$)

ρ : density($\frac{Kg}{m^3}$)

c: specific heat($\frac{Ws}{Kg°C}$)

R=$\sqrt{\xi^2 + y^2 + z^2}$: distance from the heat source to point M (m)

V_a: Traverse speed ($\frac{m}{s}$)
Q_t: Total Heat generated

6.2 Heat generation

In FSP, the heating is accomplished by friction between the tool and the workpiece and plastic deformation of workpiece. So heat is generated at or close to the contact surfaces, which have complex geometries according to the tool geometry (figure 2). For the analytical estimation, a simplified tool design with flat shoulder surface, vertical cylindrical pin side surface and a flat pin surface is assumed. The simplified tool design is presented in figure 1, where Q_1 is the heat generated under the tool shoulder, Q_2 the heat generated under the pin and Q_3 is the heat generated at the side pin surface [20].

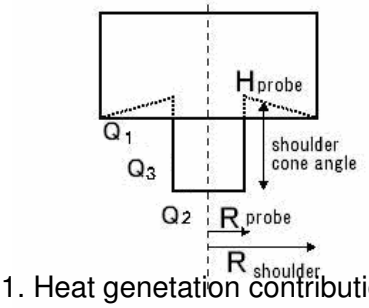

Figure 1. Heat genetation contributions [20].

Heat generated by friction [20]

The heat generated by friction between the tool and the workpiece consists of to contributions:

the heat generated under the shoulder,

$$Q_1 = \frac{2}{3}\pi\tau_{contact}\omega\left(R^3{}_{shoulder} - R^3{}_{pin}\right)$$

the heat generated under the pin,

$$Q_2 = \frac{2}{3}\pi\tau_{contact}\omega R^3{}_{pin}$$

Heat generated by plastic deformation [20]

The heat generated by plastic deformation of workpiece is the result of the shear stress due to the side pin surface,

$$Q_3 = 2\pi\tau_{contact}\omega R^2{}_{pin}H_{pin}$$

Total heat generation [20]

Hence, the total heat generation (Q_t) is the addition of Q_1, Q_2 and Q_3.

$$Q_t = Q_1+Q_2+Q_3$$

$$Q_t = \frac{2}{3}\pi\tau_{contact}\omega\left(R^3{}_{shoulder} + 3R^2{}_{pin}H_{pin}\right)$$

Contact conditions [20]

As it can be seen the total heat generation depends on the contact shear stress $\tau_{contact}$. Recently, Schmidth et al [20] have developed an analytical model for the heat generation taking into account the sticking, sliding and partial sliding/sticking contact conditions.
A contact state variable, δ, was defined. It relates the velocity of the contact points at the material surface relative to the tool point in contact.

$$\delta = \frac{v_{material}}{v_{tool}}$$

Sticking condition

The matrix closest to the tool surface sticks to it, so δ = 1. The yield shear stress τ_{yield} is estimated to be $\frac{\sigma_{yield}}{\sqrt{3}}$, where σ_{yield} is the processed material yield stress. This result is readily obtained by comparing von Mises yield criterion in uniaxial tension and pure shear. The contact shear stress is then,

$$\tau_{contact} = \tau_{yield} = \frac{\sigma_{yield}}{\sqrt{3}}$$

and the heat generation for sticking is,

$$Q_{t,sticking} = \frac{2}{3}\pi \frac{\sigma_{yield}}{\sqrt{3}} \omega\left(R^3{}_{shoulder} + 3R^2{}_{pin} H_{pin}\right)$$

Sliding condition

The tool surface and the material are sliding against each other, so δ = 0. The choice of Coulomb's friction law to describe the shear stress estimates the critical friction stress necessary for sliding condition as

$$\tau_{contact} = \tau_{friction} = \mu p$$

where μ is the friction coefficient, and p the contact pressure. Thus, the heat generation for the sliding condition is,

$$Q_{t,sliding} = \frac{2}{3}\pi \mu p\, \omega\left(R^3{}_{shoulder} + 3R^2{}_{pin} H_{pin}\right)$$

Partial sticking/sliding condition

This condition is a simple combination of the two conditions with a kind of weighting function.

$$Q_{t,sticking/sliding} = \delta Q_{t,sticking} + (1-\delta) Q_{t,sliding}$$

$$Q_{t,sticking/sliding} = \delta \frac{2}{3}\pi \frac{\sigma_{yield}}{\sqrt{3}} \omega\left(R^3{}_{shoulder} + 3R^2{}_{pin} H_{pin}\right) + (1-\delta)$$
$$\frac{2}{3}\pi \mu p\, \omega\left(R^3{}_{shoulder} + 3R^2{}_{pin} H_{pin}\right)$$

In the present work, the sticking condition will be used.

Heat losses

Only a part of the heat generated plays a direct role in the process, the other part is lost. The heat losses are classified in three terms: conduction heat losses through the tool, conduction heat losses through the montage and convection heat losses through the air.

In summary, many factors influence the thermal profiles during FSP. First, tool shoulder dominates heat generation during the process. Second, maximum temperature increases with increasing tool rotation rate at a constant tool traverse speed and decreases with increasing traverse speed at a constant tool rotation rate. Furthermore, maximum temperature during FSP increases with increasing the ratio of tool rotation rate/traverse speed.

Finally, it can be concluded that quality of processed zones strongly depends on tool rotation rate and traverse speed. Usually, tool rotation rates really higher than tool traverse speeds (w>>v) leads to a lack of stirring and mixing. On the contrary, tool traverse speeds really higher than tool rotation rates (w<<v) leads to a sound increase in temperature. Optimization of tool rotation rate and traverse speed will provide the sufficient processing temperature for an optimal stirring and mixing action without heating too much.

7. RECRYSTALLIZATION

Recrystallization in the mechanism by which strained grains of cold-worked metal are replaced, upon heating, by more regularly-spaced grains. This occurs through short-range diffusion enabled by the high temperature [21].

Generally, grains evolve according to two different ways: static and dynamic. Static recrystallization SRX occurs when a hot deformed material is subsequently annealed. In contrast, dynamic recrystallization DRX occurs during deformation [21].

Aluminium and its alloys are generally noted for dynamic recovery (DRV) during hot deformation to such a high level that they typically do not undergo dynamic recrystallization (DRX). This is generally attributed to the high stacking fault energy of aluminium, which makes dislocation climb and cross slip easy. As a result is difficult to achieve a sufficiently high dislocation density to initiate and sustain DRX. As an exception, DRX has been reported in Al of extremely high purity; this is attributed to the very high grain boundary mobility in this material.

During Friction Stir Processing, the material which flows around the tool undergoes intense plastic deformation at elevated temperature, normally leading to a very fine grain structure in the centre of the processed zone.

Although it is not clear which kind of recrystallization is involved in the process the final fine equiaxed grained microstructure obtained is supposed to be attributed to DRX.

Generally, two types of DRX are discussed: continuous DRX and discontinuous DRX. During continuous dynamic recystallization subgrains rotate and achieve a high angle misorientation. In contrast, during discontinuous DRX new grains exhibiting large-angle boundaries evolve, e.g. dynamic nucleation followed by grain growth from migration of large-angle boundaries [21].

Several researchers have proposed continuous dynamic recystallization by rotation of existing subgrains [22] or subgrains developed during processing within the parent microstructure [23].

Jata and Semiantin [22] suggested that the original parent metal low-angle boundaries are replaced by high-angle boundaries by continuous rotation of the low-angle boundaries during FSP. Dislocation glide gives rise to a gradual relative rotation of adjacent subgrains. However, many of the recrystallized grains formed in the DRX are finer than the original subgrain size. Thus, it is unlikely that the recrystallized grains in dynamic recrystallization zone are the result of the rotation of original subgrains in the base metal.

Su et al, in its early study [23], presented DRX in the dynamic recrystalliized zone as a continuous DRX process based on dynamic recovery. Subgrain growth associated with repeated absorption of dislocations into the boundaries is the recristallization mechanism.
The authors proposed that the evolution of the dynamic recrystallization process in the dynamic recrystallization zone undergoes the following paths:

Dislocation introduction: In the early stage of the thermal-mechanical cycle a large amount of lattice dislocations are introduced by plastic deformation while at the same time growth occurs as a result of the elevated temperature produced by FSP.

Dynamic recovery: Many subgrains are formed intragranularly by dislocation motion. The subgrains are very small and exhibit low-angle boundaries.

Continuous dynamic recrystallization: During the subsequent thermal-mechanical deformation, dislocations are introduced continuously in the subgrains to accommodate the strain incompatibility of neighbouring subgrains. The small subgrains grow and rotate by repeated absorption of the accommodating dislocations into the subgrain boundaries, resulting in formation of the equiaxed grains with high-angle boundaries.

Repeated introduction of dislocations and partial recovery: After dynamic recrystallization, plastic deformation generates additional dislocations within the recrystallized grains. At the end of the thermal-mechanical cycle, partial recovery occurs.

In a recent study Su et al [24] demonstrated that the small grains within the friction stir processed zone are not subgrains but new grains separated by high-angle boundaries. Recently, nanocrystalline 7075 Al was successfully obtained [23]. In their opinion, the formation of such small grains can not be explained by conventional mechanisms. It is hard to believe that subgrains even smaller than nanocrystals can be formed at high temperature during FSP. The authors believe that the very small grain structures formed around the pin tool are the result of discontinuous DRX under very large strain and very high strain rate at high temperature. However, the mechanism and the kinetics of the process are not clear because is not a conventional discontinuous DRX with dynamic nucleation (dynamic recovery and grain coarsening).
The authors propose that apart from discontinuous DRX other mechanisms such as DRV and continuous DRX act at different stages of the microstructure evolution in friction stir processed zone.

To find out the exact mechanisms for such microstructural evolution they analysed some samples cut from different regions behind the pin tool, as illustrated in Figure 1.

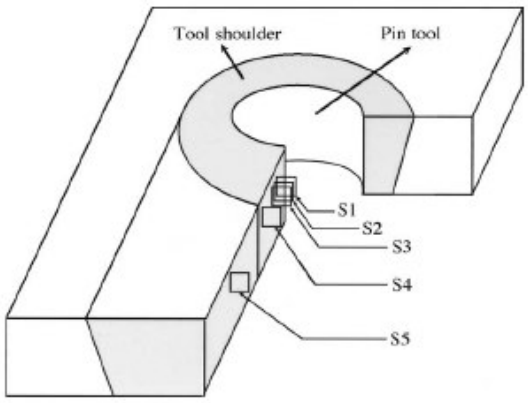

Fig 1 Microstructure evolution during FSW/FSP of high strength aluminium alloys [24].

In specimen 1, very small grains were formed around the pin tool by dynamic recristallization (DRX) at elevated temperatures. The grain boundaries evolved by absorption of numerous dislocations provided by the surrounding structure, and additional dislocations were generated by subsequent plastic deformation in the larger grains, which accommodate strains preferentially.

Specimen 2 showed how the small grains formed in the initial stages of Friction Stir Processing coarsen, and additional dislocations were introduced during subsequent thermal-mechanical deformation. Furthermore, dynamic recovery occurred in some of the grains.

During continued processing, specimen 3 grain size increased. Most of the grains contained dislocations, but had different dislocation densities even in grains of similar size, whereas some grains were almost free of dislocations. There were grains in process of recovery, adjacent to the grains that exhibited a high dislocation density. It was also noted that grains within different stages of recovery existed next to each other.
The observed dislocation density differences could not be attributed to differences in thermal cycles because of the high thermal conductivity of aluminium alloys. Therefore, it was likely that deformation gradients existed across the grains during the processing operation.

Grains in specimen 4 shared similar dislocation and recovery structures with the grains in specimen 3. Furthermore, the grain size was only slightly larger than of the specimen 3, suggesting a decrease in grain growth rate with increase in distance from the pin tool.

Specimen 5 exhibited a recrystallized, fine equiaxed grain structure separated by high-angle boundaries. A variety of dislocation structures were observed in the recrystallized grains. Some grains contained a low density of dislocations while a high density of dislocations was observed in many grains. There were also grains with different degrees of recovery. Furthermore, some dislocations aligned to form subgrain boundaries and subsequent dislocation absorption into subgrain boundaries was present. These microstructural characteristics suggest that the subgrains formed by dynamic recovery (DRV) evolved by a mechanism of continuous DRX.

This study suggested that, due to non-uniform plastic deformation introduced in recystallized grains, the final microstuctures in FSP consists of some grains that are result of growth of initial recrystallized grains while others are formed from subgrains via continuous dynamic recrystallization.

Such microstructure observation revealed a complex process of microstructure evolution during Friction Stir Processing presented in schematic illustration at fig 2.

Two possible recystallization models, model 1 and 2 are presented.

Model 1 includes discontinuous dynamic recrystallization, grain growth and dislocation introduction. Therefore, model 1 leads to a final equiaxed microstructure with a high density of dislocations.

Model 2 includes discontinuous dynamic recrystallization, dynamic recovery and continuous dynamic recrystallization. Thus, in model 2 low densities of dislocations are expected.

Figure 2 shows the microstructure evolution during FSW/FSP of high strength aluminium alloys.

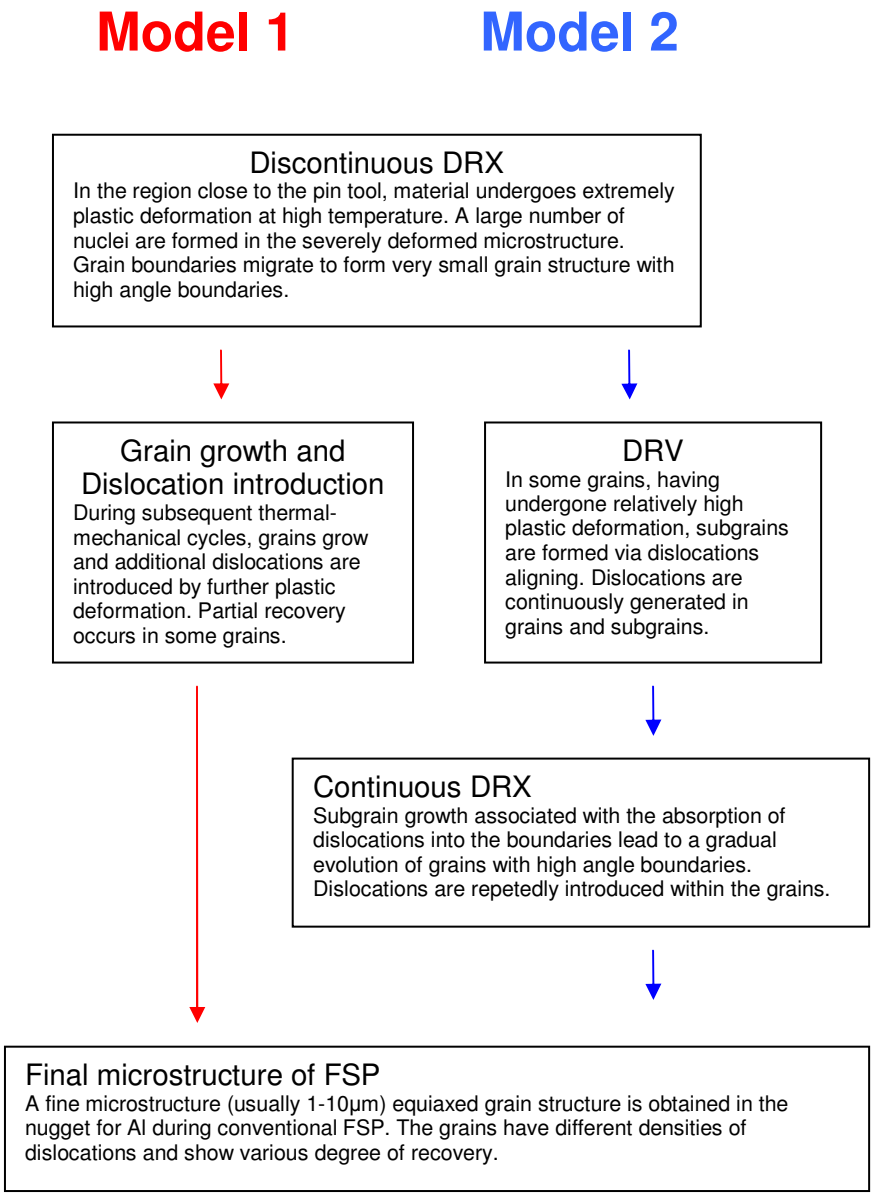

Figure 2. Microstructure evolution during FSW/FSP of high strength Al alloys [24]

The present schema reveals a varied recrystallization mechanism in Al alloys during FSP. It is apparent that the recrystallization mechanisms acting at different stages of the microstructure evolution are related to the strain, strain rate and the thermal cycle of the material undergone at each stage.

8. ALLOYS STUDIED : Al 1050 and A365

8.1 Aluminium

Pure aluminium is a soft lightweight metal. Mixed with small, often minute, quantities of other materials – iron, silicon, zinc, copper, magnesium, tin, titanium, lithium, chromium, tungsten, manganese, nickel, zirconium and boron - it is possible to produce an array of alloys with specific properties for very different purposes. Strength depends on purity. 99.996 per cent pure aluminium has a tensile strength of about 49 MPa, rising to 700 MPa following alloying and suitable heat treatment.

Aluminium can be strong, light (less than one third the specific weight of steel, copper or brass), ductile, and malleable. It is an excellent conductor of heat and electricity. It resists corrosion and it can be recycled – again and again and again, with no loss of quality or properties. Polished aluminium has the highest reflectivity of any material - even mirror glass.

Aluminium's range of properties can be found in an impressive array of commercially available alloys. The composition and logic of those alloys are regulated by an internationally agreed classifications system or nomenclature for wrought and as-cast aluminium alloys.

Alloys fall into three main groups:

- The wrought work-hardening alloys, where strength is achieved by the amount of cold work applied to the alloy, e.g. by rolling.
- The wrought heat-treatable or precipitation hardening alloys, where the strength and properties are achieved by heat treatments of varying complexity
- As-cast aluminium alloys.

The wrought and as-cast scheme is as follows (Table1). Each registered alloy is described by a four digit number. The classification provides for:

Major Alloying Element	Wrought	As-cast
None (99%+ Aluminium)	1XXX	1XXX0
Copper	2XXX	2XXX0
Manganese	3XXX	
Silicon	4XXX	4XXX0
Magnesium	5XXX	5XXX0
Magnesium + Silicon	6XXX	6XXX0
Zinc	7XXX	7XXX0
Lithium	8XXX	
Unused		9XXX0

Table 1. Designations for alloyed wrought and as-cast aluminium alloys.

8.2 Al 1050

Al 1050 is a minimum 99% purity aluminium alloy. The chemical composition is as follows (Table2):

Element	% Present
Cu	0.05%
Mg	0.05%
Si	0.25%
Fe	0.4%
Mn	0.05%
Zn	0.07%
Ti	0.05%
Al	Balance

Table 2. Typical chemical composition for aluminium alloy 1050

As a wrought work-hardening alloy, the 1050 aluminium alloy has their properties adjusted by cold work, usually by cold rolling.

The properties of this aluminium of 99% purity alloy depend upon the degree of cold work and whether any annealing or stabilising thermal treatment follows the cold work. A standardised nomenclature is used to describe these conditions.

It uses a letter, O, F or H followed by one or more numbers. It is presented in summary form in Table 3 and defined in Table 4.

New Symbol	Description
O	Annealed, soft
F	As fabricated
H12	Strain-hardened, quarter hard
H14	Strain-hardened, half hard
H16	Strain-hardened, three quarter hard
H18	Strain-hardened, fully hard
H22	Strain-hardened, partially annealed quarter hard
H24	Strain-hardened, partially annealed half hard
H26	Strain-hardened, partially annealed three quarter hard
H28	Strain-hardened, partially annealed fully hard
H32	Strain-hardened and stabilised, quarter hard
H34	Strain-hardened and stabilised, half hard
H36	Strain-hardened and stabilised, three quarter hard
H38	Strain-hardened and stabilised, fully hard

Table 3. Standard nomenclature for work hardened aluminium alloys.

Term	Description
Cold Work	The nomenclature denotes the degree of cold work imposed on the metal by using the letter H followed by numbers. The first number indicates how the temper is achieved.
H1x	Strain-hardened only to obtain the desired strength without supplementary thermal treatment.
H2x	Strain-hardened and partially annealed. These designations apply to products which are strain-hardened more than the desired final amount and then reduced in strength to the desired level by partial annealing. For alloys that age-soften at room temperature, the H2x tempers have the same minimum ultimate tensile strength as the corresponding H3x

	tempers. For other alloys, the H2x tempers have the same minimum ultimate tensile strength as the corresponding H1x tempers and slightly higher elongation.
H3x	Strain-hardened and stabilised. These designations apply to products which are strain-hardened and whose mechanical properties are stabilised either by a low temperature thermal treatment or as a result of heat introduced during fabrication. Stabilisation usually improves ductility. This designation is applicable only to those alloys which, unless stabilised , gradually age soften at room temperature.
H4x	H4x Strain-hardened and lacquered or painted. These designations apply to products which are strain-hardened and which may be subjected to some partial annealing during the thermal curing which follows the painting or lacquering operation. The second number after H indicates the final degree of strain-hardening, number 8 being the hardest normally indicated. The third digit after H, when used, indicates a variation of a two digit temper. It is used when the degree of control of temper or the mechanical properties or both differ from, but are close to, that (or those) for the two digit H temper designation to which it is added, or when some other characteristic is significantly affected. The fully soft annealed condition is indicated by the letter O and the `as fabricated' ie material that has received no subsequent treatment is indicated as F. To illustrate; it can be seen that 3103-0 denotes a particular aluminium manganese alloy in the annealed, soft condition, whilst 3103-H16 denotes the same alloy strain-hardened to three quarters hard.

Table 4. Explanations of symbols used in table 4.

Alloy 1050 is most commonly supplied in sheet form with a H14 temper. H14 refers to work hardening of the alloy to a half hard temper.

In the present work the aluminium alloy Al 1050-H14 was heat treated during 1 hour at 570℃. After the heat treatment the alloy in the annealed condition (Al 1050-O) was obtained. The microstructure had changed. The alloy Al 1050-H14 showed elongated grains to the rolling direction. In contrast, the Al 1050-O annealed alloy consisted of equiaxed grains of 35-45 μm diameter size. The picture below shows the obtained microstructure (Figure 1). This microstructure results in a reduction of its mechanical property levels to their minimums (dead soft). Aluminium alloy 1050-O consists in maximum plasticity and minimum tensile strength.

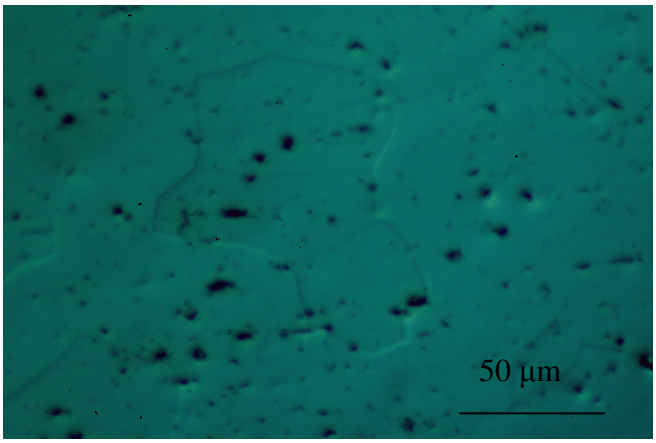

Figure 1. Al 1050-O microstructure

Some of its properties are attached in the tables below. Table 5 and 6 describes the typical mechanical and physical properties respectively.

Proof Stress 0.2% (MPa)	35
Tensile Strength (MPa)	80
Elongation A5 (%)	42
Hardness Vickers (HV)	20-25

Table 5. Typical mechanical properties for aluminium alloy 1050-O

Property	Value
Density	2.71 g/cm^3
Melting Point	650℃
Modulus of Elasticity	71 GPa
Electrical Resistivity	0.0282x10^{-6} Ω.m
Thermal Conductivity	222 W/m.K
Thermal Expansion	24x10^{-6} /K

Table 6. Typical physical properties for aluminium alloy 1050-O

The properties showed above have a sound influence in the fabrication response. The typical fabrication response figures in table 7.

Process	Rating
Workability – Cold	Excellent
Machinability	Poor
Weldability – Gas	Excellent
Weldability – Arc	Excellent
Weldability – Resistance	Excellent
Brazability	Excellent
Solderability	Excellent

Table 7. Typical fabrication response for aluminium alloy 1050-O

Thanks to that fabrication response, some applications of Al 1050 are:

- Chemical process plant equipment
- Food industry containers
- Pyrotechnic powder
- Architectural flashings
- Lamp reflectors
- Cable sheathing

8.3 A356

However versatile the processes used to obtain wrought alloys provides only two dimensional shapes. Casting on the other hand allows complex three dimensional products to be made. Sand permanent mould and die casting techniques are all

employed. The choice of process depends upon quantity of castings required, end use and quality and property considerations.

Silicon is a good alloying element in metallic aluminium alloys used for casting. This is because it increases the fluidity of the melt, reduces the melting temperature, decreases the contraction associated with solidification and is very cheap as a raw material. Silicon also has a low density, which may be an advantage in reducing the overall weight of the cast component. Silicon has a very low solubility in aluminium; it therefore precipitates as virtually pure silicon, which is hard and hence improves the abrasion resistance.
Magnesium provides strength while maintaining reasonable ductility.

In the present work as-cast A356 having the composition A356 - nominally 7% silicon, 0.35% magnesium is used.

From the phase diagram can be considered a hypoeutectic aluminium-silicon alloy with the following microstructure (Figure 2).

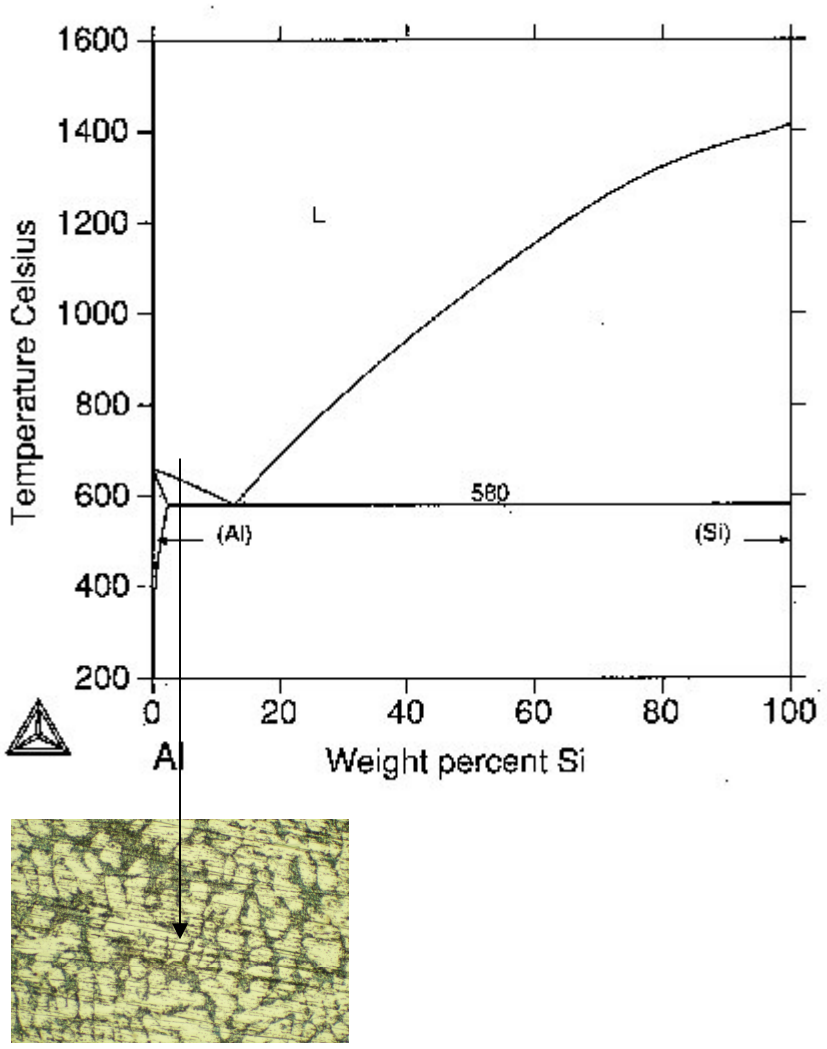

Figure 2. Phase diagram and aluminium-silicon casting alloy 7% silicon microstructure

The picture in figure 2 shows the microstructure of the as-cast A356 used. The microstructure consists of primary α-aluminium dendrites and interdendritic irregular Al-Si eutectic regions.

This microstructure has a sound influence in its mechanical properties. Some of them are attached in the table 8:

Proof Stress 0.2% (MPa)	80
Tensile Strength (MPa)	180
Elongation A5 (%)	5
Hardness Vickers (HV)	60-65

Table 8. Typical mechanical properties for as-cast A356

Some important applications of aluminium-silicon casting alloys are:

- Lightweight components for vehicles, aircraft, ships and spacecraft.
- General engineering components where light weight and corrosion resistance are required.
- Architectural fittings where light weight and good appearance are important.
- High-tech products for office and home.

9. STRENGTHENING MECHANISMS

Pure, untreated aluminium is a soft metal with insufficient strength for most engineering applications. In order to take advantage of its low density, aluminium has to be strengthened. To increase the strength of metals it is necessary to impede the movement of dislocations.

In general, four different strengthening mechanisms are used to strengthen aluminium. These are summarised below:

Mechanism	Description	Dislocation barrier
Strain hardening	Plastic deformation, or work hardening, of metals increases the dislocation density. Dense dislocation 'tangles' can form, obstructing the movement of other dislocations.	Other dislocations
Solute hardening	Alloy elements, such as Mg, Mn and Cu can 'pin' dislocations, thereby strengthening the material.	Solute atoms
Precipitation hardening	Small, finely dispersed precipitates can significantly increase the strength of aluminium alloys.	Precipitates
Grain size hardening	Reducing the grain size increases the alloy strength according to the Hall-Petch relationship.	Grain boundaries

During Friction Stir Processing, the material which flows around the tool undergoes intense plastic deformation at elevated temperature, normally leading to a very fine grain structure with different densities of dislocations and various degrees of deformation. Thus, it is believed that two of those strengthening mechanisms, in particulary, grain size hardening and strain hardening, are involved in the process.

The third part of the present work will be focused on the effect that those two mechanisms have on the hardness improvement of Al 1050-0.

9.1 Strain Hardening

Ductile metals become stronger when they are deformed plastically at temperatures below the melting point. Such plastic deformation involves a multiplication of dislocations. Thus, the average distance between dislocations decreases and dislocations start blocking the motion of each other increasing the strength of the metal.

FSP involves plastic deformation at which the multiplication of dislocations occurs. If the multiplication of dislocations occurs at a faster rate than they are annihilated by dynamic recovery (Heating - increased diffusion - enhanced dislocation motion) the strengthening effect is assured. Otherwise, if the contrary happens, a so sound strengthening effect won't be expected.

9.2 Grain size hardening

Strengthening by Grain Size Reduction is based on the fact that it is difficult for a dislocation to pass into another grain, especially if it is very misaligned. Atomic disorder at the boundary causes discontinuity in slip planes. High-angle grain boundaries block slip and increase strength of the material. A stress concentration at end of a slip plane may trigger new dislocations in an adjacent grain. Small angle grain boundaries are not effective in blocking dislocations.
The finer the grains the larger the area of grain boundaries that impedes dislocation motion.

Usually, the yield strength varies with grain size, d, according to Hall-Petch equation (Equation 1) [15].

$$\sigma_y = \sigma_o + K_y d^{-1/2}$$

Equation 1. Hall-Petch relationship (Yield Stress) [15]

where σ_o and K_y are constants for a particular material, and d is the average grain diameter.

This relationship serves to demonstrate that yield stress increases with decreasing grain size.

In the absence of appreciable work hardening, the hardness of the material is proportional to yield stress through the expression $Hv \sim 3\sigma_y$. Equation 1 is therefore reformulated in terms of hardness through the following relationship Equation 2 [15]:

$$H_v = H_o + K_H d^{-1/2}$$

Equation 2. Hall-Petch relationship (Hardness) [15]

where H_o and K_H are the appropriate constants associated with the hardness measurements.

FSP results in a fine grain microstructure. Thus, from the Hall-Petch relationship, an increase in hardness is expected due to such grain refinement. Unfortunately, for aluminium, a sound decrease in the grain size does not represent a sound increase in yield strength. This means that the hardness increase of Al 1050-O could not be only explained by the grain size hardening mechanism. Therefore, strain hardening mechanism must play an important role in hardness increase. Figure 1 show the Hall-Petch relationship for several metals

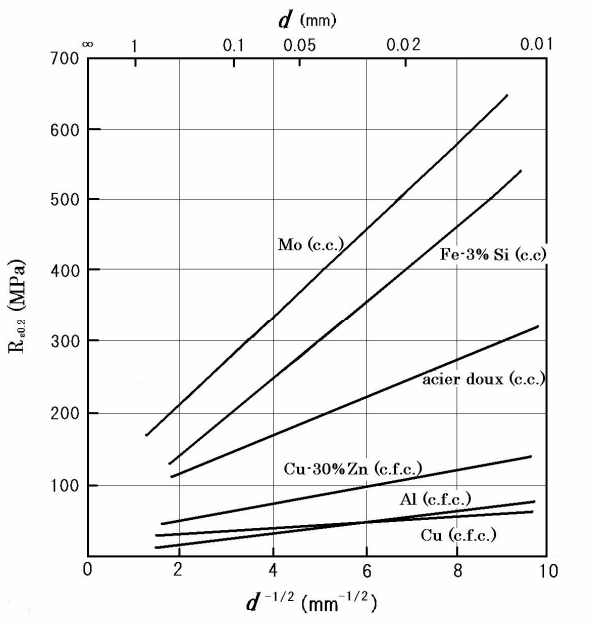

Figure 1. Hall-Petch relationship.

10. MICROSTRUCTURE IMPROVEMENT OF A356

10.1 Introduction

An essential strategy for reducing weight in transportation industry is increasing the use of lightweight materials such as aluminium. So, aluminium foundry alloys are in high demand as an engineering material. Using aluminium castings to replace iron castings will result in cutting the component weight by half. Typically, aluminium castings contain porosity, segregated chemistries, and inhomogeneous microstructures. These undesirable features result in property degradation including reduced strength and ductility, poor corrosion resistance, and limited fatigue life.

Al-7wt.%Si-Mg alloys with Mg contents in the range of 0.25 to 0.65 wt% (A356 and A319) are widely used to cast high-strength components in the aerospace and automobile industries because they offer a combination of high achievable strength with good casting characteristics. The silicon gives good fluidity when casting, enabling thin sections to be successfully cast. The magnesium provides strength while maintaining reasonable ductility.
However, the mechanical properties of such cast hypoeutectic aluminium alloys, in particular strength and ductility, are limited by three drawbacks, i.e., porosity, coarse acircular Si particles, and coarse primary aluminium dendrites.

In the past two decades, various modification and heat-treatment techniques have been developed to refine the microstructure of cast Al-Si alloys.
The first category of research is aimed at modifying the morphology of Si particles to fine and globular particles. Chemical modification methods involve adding very small amounts of sodium, strontium, or antimony, known as eutectic modifiers. Thermal modification involves heat-treatment of cast alloys at high temperature, usually at the solid solution temperature around 540 ℃ for long times.
The second research category refines the coarse primary aluminium phases. A heat treatment at an extremely high temperature of 577 ℃ for a short time resulted in a substantial refinement in the aluminium dendrites.

None of the modification and heat-treatment techniques mentioned above can eliminate the porosity effectively and redistribute the Si particles uniformly into the aluminium matrix.

Therefore, a more effective modification technique is highly desirable for microstructural modification of A356 and A319 alloys to enhance mechanical properties, in particular, ductility [8,10,11].

Friction Stir Processing, as a new solid state processing technique for microstructural modification in metallic materials has been applied to A356.

10.2 Experimental Procedures

A356 cast plates having the dimensions of 200 x 80 x 6,5 mm were used for FSP. The nominal composition was reported in Alloys studied paragraph.
Single pass FSP was performed using a tool with large diameter shoulder and a consaped pin. Diameter shoulder was 20 mm, bigger diameter pin was 6 mm, smaller diameter pin was 3 mm and pin length was 4 mm. Figure 1 shows the tool used.

Figure 1. Tool used.

The tool rotation rate was 900 rpm and the tool traverse speed 1 mm/s. These conditions were used to make stir passes with lengths of about 190 mm. As-processed plates were cut in a rectangular shape having dimensions of 40 x 12 x 6,5 mm transverse to the processing direction. Figure 2 presents a cross section perpendicular to the processed zone.

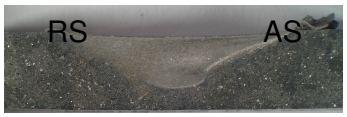

Figure 2. Cross section perpendicular to the processed zone.

Afterwards, they were grinded using silicon carbide paper (220, 320, 500 and 1000) and polished with 6 μm diamond DP-suspension. Electropolishing was also applied.

Microstructural examination was presented using an optical microscopy under polarized light. The samples for optical microscopy where etched using HF 0.5% during at least 10 min.

To evaluate the effect of FSP on the properties of A356, Vickers microhardness testing and tensile testing were performed.
Vickers hardness profiles were measured on the cross-section presented above (Figure 2). The microhardness measurements were made on the metallographically prepared specimens. The indentations were made under a 200 g load extending from the processed zone into the base metal.
Tensile specimens were machined in both the traverse and longitudinal direction from the FSP region. The traverse direction sample was used for the tensile properties characterization of the base material. The longitudinal direction sample was used for the tensile properties characterization of the processed zone. Figure 3 shows the tensile specimens machined.

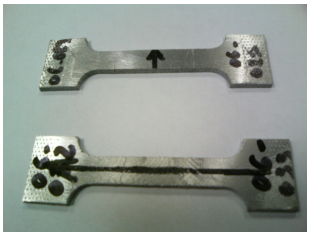

Figure 3. Tensile specimens machined.

10.3 Results and discussion

Microstructure

Figure 4 shows the macrostructure of the Friction stir processed zone and Figures 5-7 illustrate details of the variation of the microstructure corresponding to the regimes indicated by a-d in figure 4. The microstructure of the processed zone is formally divided into three areas: base metal (a), the nugget zone (b) and thermo-mechanically affected zone (TMAZ) (d and c).

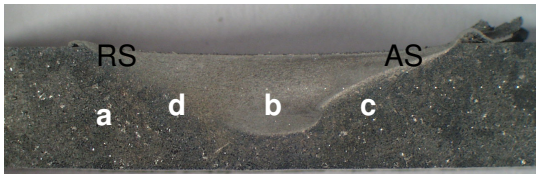

Figure 4. Macrostructure of the A356 Friction stir processed zone.

Figure 5 shows the microstructure of the base metal (a).

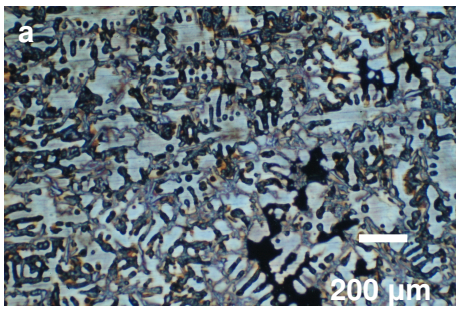

Figure 5 Microstructure of the A356 base metal.

The microstructure of as-cast A356 consists of primary aluminium dendrites and interdendritic irregular Al-Si eutectic regions. The average grain size was approximately 100 µm. Furthermore, porosity of ~ 50 µm diameter was detected.

Figure 6 shows the microstructure of FSP A356 in the central nugget zone (b).

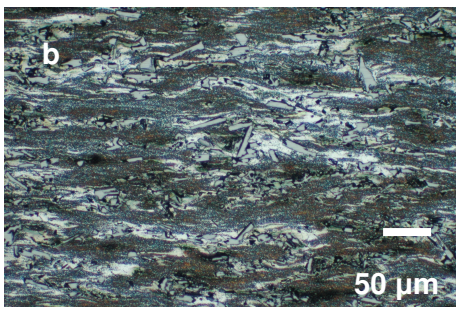

Figure 6. Nugget zone microstructure of FSP A356.

FSP resulted in a fine Si particles uniformly distributed in the aluminium matrix due to the intense breakup of the as-cast microstructure and subsequent material mixing. As seen in figure 5 grain boundaries are hard to distinguish in FSP A356. However, the grain size in the present FSP A356 is estimated to be on the order of ~3 µm. Moreover, porosity in the as-cast A356 was nearly eliminated by FSP.

Figure 7 shows the microstructure of the TMAZ (c and d). In other words, shows the boundary between the base metal and the FSP zone.

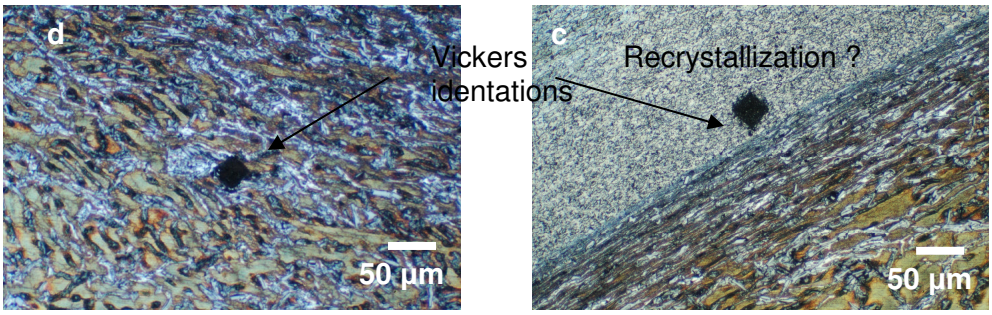

Figure 7. Microstructure of the TMAZ A365 FSP: c) advancing side and d) retreating side.

The TMAZ microstructure consists of bent elongated grains near the nugget shown in the micrograph (c) and (d), and divided into the retreating side (RS) (Figure 7c) and the advancing side (AS) (Figure 7d) depending on different microstructures. Although both the advancing side and the retreating side have a boundary with the processed zone, the boundary in the advancing side is clearer than that in the retreating side. This phenomena is due to the different material flow in both sides.

It's worth pointing out that in the nugget of the advancing side boundary, a recystallization phenomena seems to be presented. No other recent studies talk about recrystallization in as cast FSP. Further work is needed, but such recystallization is attributed to the temperature reached in this zone which seems to be closed to the eutectic.

As seen in the optical micrographs, FSP, generally, break up and disperse the coarse acircular SI particles creating a uniform distribution of Si particles in the aluminium matrix. Further, FSP healed the porosity. A recrystallization phenomena in the nugget of the advancing side is presented.

Hardness Profiles

The effect of friction stir processing on the distribution of hardness on the A356 is illustrated in Figure 8.

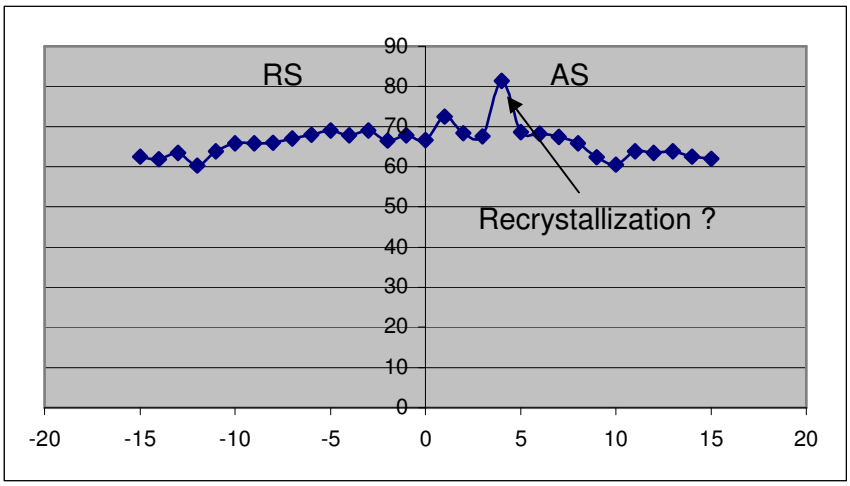

Figure 8. Hardness Profile of FSP A365.

The results show a slightly hardening effect in A356 friction stir processed zone (Base metal hardness 65 Hv). This is consistent with its more uniform microstructure. Soft spots found in the casting due to porosity and Al dendrite cores were eliminated by the friction stir processing.
It's worth notting that the high hardness value point (81,4 Hv) reached in the nugget of the advancing side zone (4 mm) corresponds to the recrystallization phenomena presented.

Tensile Properties

In some recent studies [8,10,11] was probed that A356 FSP resulted in a significant improvement in tensile properties, particularly the ductility. Figure 9 shows how friction stir processing increased total uniform elongation values in A356 from under 3% to over 12%.

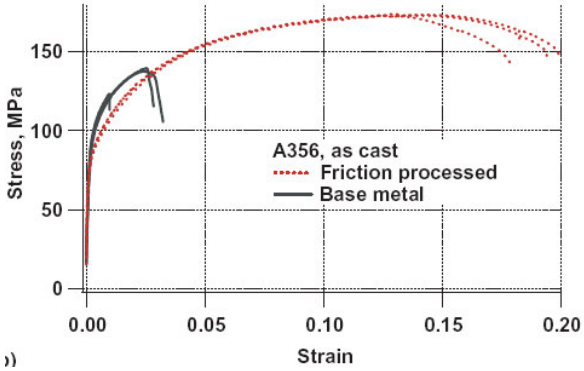

Figure 9. Stress-Strain plot for A365 FSP [10].

Generally ultimate tensile strengths and ductilities improve as porosity levels and microstructure scale decreases. The tensile behaviour of the FSP A356 is consistent with this behaviour patern.

In the present work the demonstration of the large ductility increase for friction stir processed A356 was attempted but no achieved. Figure 10 shows the stress-strain plots from room temperature tensile tests done on friction stir processed A356.

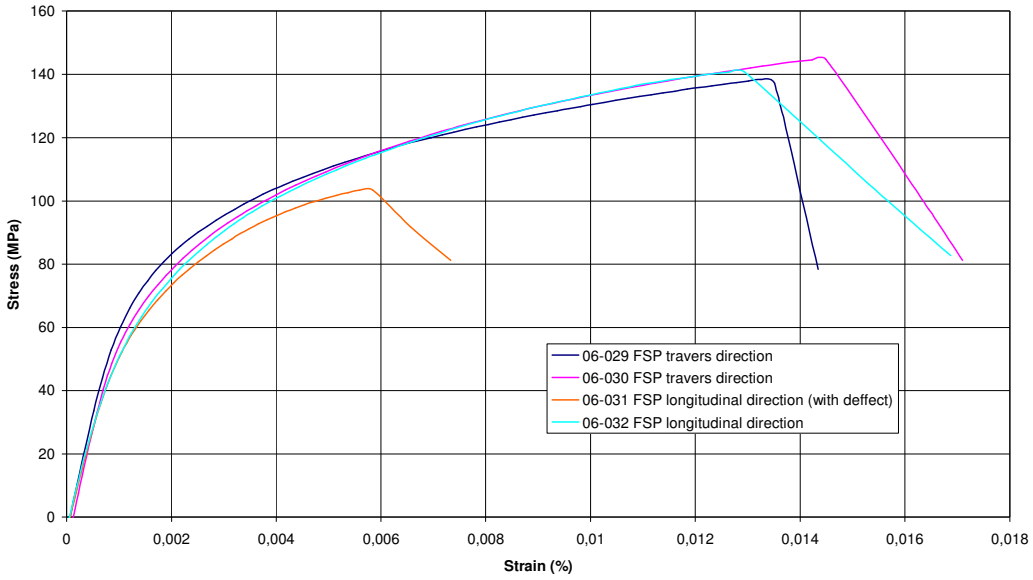

Figure 10. Stress-Strain plots for A365 FSP.

From the graphic above no increment on ductility in FSP A356 is presented.

Tensile specimens machined in the traverse direction (06-029 and 06-030) from the FSP region, broke in the base metal zone. So the stress-strain values reached represent the base material ultimate tensile strength and ductility.
Tensile specimens machined in the longitudinal direction (06-031 and 06-032) from the FSP region, were entirely composed by friction stir processed A356. Specimen 06-031 broke at stress-strain values lower than the base material ones due to a defect presented in the whole friction stir processed zone. Specimen 06-032 broke at stress-strain values similar to the base material ones. Table 1 shows a comparison of tensile properties for the as-cast and friction stir processed A365.

Condition	Specimen nº	Tensile Strength (Mpa)	Strain (%)
as-cast	06-029	138	0,013
	06-030	145	0,015
FSP	06-031	104	0,006
	06-032	141	0,013

Table 1. Tensile properties for the as-cast and friction stir processed A365.

From the data, similar tensile strength between as-cast and FSP A365 was demonstrated. Tensile strength was even slightly higher in 06-032 specimen than 06-029 specimen as the hardness profiles indicated. However, no increment on ductility could be probed on FSP A365. Maybe, tensile specimens were machined in a bad way so they broke before they would do.

10.4 Conclusions

FSP created a fine and uniform microstructure in as-cast A356. The stirring action closed porosity, fractured large second-phase particles, and uniformly distributed particles throughout the stir zone microstructure. The elimination of porosity, the significant microstructural refinement, and homogenization caused a slightly improvement in mechanical properties of FSP A356 such as hardness and ultimate tensile strength. Unfortunately ductility improvement could not be probed.

11. MICROSTRUCTURE IMPROVEMENT OF Al 1050-0 FUSION WELD

11.1 Introduction

The welding of aluminium and its alloys has always represented a great challenge for designers and technologists. Traditional fusion welding processes such as inert-gas metal-arc welding (MIG) and tungsten-arc welding (TIG) when applied to several aluminium alloys, present lots of difficulties that have sometimes discouraged the use of such kinds of welded materials. Such difficulties are mainly related to the presence of a tenacious oxide layer, high thermal conductivity, high coefficient of thermal expansion, solidification shrinkage and high solubility of hydrogen, and other gases, in molten state. As a consequence of all above-mentioned problems, Friction Stir Welding (FSW) is a solid state joining method particularly well suited to aluminium alloys, which are often difficult to fusion weld without hot cracking, porosity or distortion. The resulting joint is superior to that of a traditional fusion weld in that it has lower residual stresses, and is free of the cast microstructure and defects such as cracking and porosity.
However, it will not be possible to friction stir weld all aluminium structures and reap the benefits of this solid state process. For example, large structures, inaccessible locations, and very thick plate would be difficult to friction stir weld. However, eventually it may be possible to friction stir process the surface of fusion welds. By friction stir processing the surface, the fusion weld microstructure will be converted to a fully recrystallized fine grain and weld defects near the surface will be eliminated.

The present study revealed that FSP applied to a fusion weld such as TIG results in a sound change of microstructure similar to the one expected in FSW applied to the starting material.

11.2 Experimental Procedures

The starting material used in this study was Al alloy 1050-O. As reported in the Alloys Studied paragraph, the chemical composition was Al-0.25Si-0.4Fe-0.05Cu-0.05Mg-0.05Mn-0.07Zn-0.02Ti (all compositions are in wt.%). The average grain size was about 45 μm and the hardness value was approximately 21 HV. A rectangular plate having dimensions of 200 x 80 x 6 mm was prepared from the sheet of starting material. TIG welds and subsequent FSP were applied to the 1050 Al plate.
TIG was performed with no filler material in Ar atmosphere. The travelling speed was 2.5 mm/s. The intensity was 200 A. Two fusion welds toes, one beside the other, were performed. Schematic illustration of the two fusion weld toes are shown in figure 1.

Figure 1. Schematic illustration of the two fusion weld toes.

FSP was performed using a tool with large diameter shoulder and a customized pin with a shorter length. This larger diameter shoulder tool was designed for a single pass across the entire fusion weld crown. Diameter shoulder was 20 mm, diameter pin was 10 mm and pin length was 1 mm. Figure 2 shows the tool used.

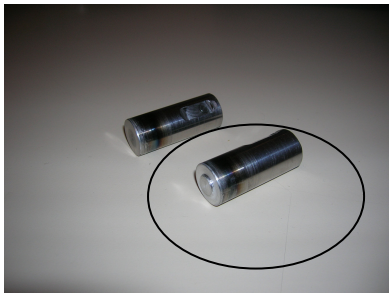

Figure 2. Tool used

The tool rotation rate was 500 rpm and the tool traverse speed 1 mm/s. These conditions were used to make single stir passes with lengths of about 200 mm. Figure 3 presents a cross section perpendicular to the processed zone.

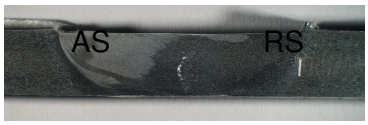

Figure 3. Cross section perpendicular of the processed zone.

Following the processes, Vickers hardness profiles were measured on the cross-section presented above. The microhardness measurements were made on metallographically prepared specimens. The specimens were cut in a rectangular shape having dimensions of 40 x 12 x 6 mm. After, they were grinded using silicon carbide paper (220, 320, 500 and 1000) and polished with 6 μm diamond DP-suspension. Electropolishing was also applied. The indentations were made under a 50 g load extending from the processed zone into the base metal.

Grain structures in the processed zones were observed by optical microscopy under polarized light. The samples for optical microscopy where etched using HF 0.5% during at least 10 min.

11.3 Results and discussion

Microstructure

Figure 4 shows the macrostructure of the fusion weld toes. The microstructure shows the typical cast weld microstructure. Figure 5 illustrates details of the variation of the microstructure corresponding to the regimes indicated by a-c in figure 5. The microstructure of the welded zone is formally divided into three areas: base metal, heat affected zone and the fusion zone.

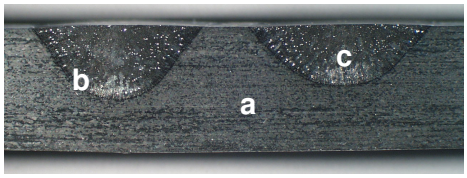

Figure 4. Macrostructure of the fusion weld toes.

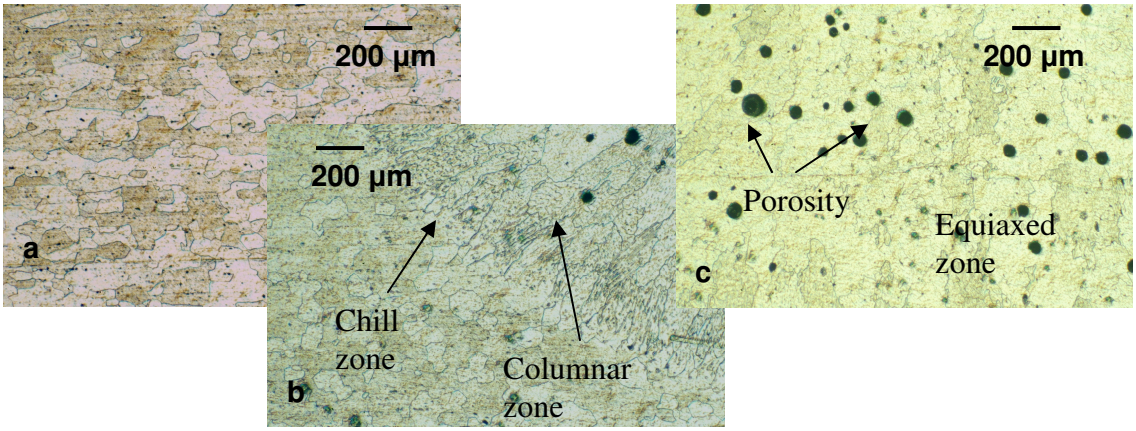

Figure 5. Microstructure variation of the fusion weld toes: a) base metal, b) heat affected zone and c) fusion zone.

The fusion zone (c) represents the metal melted during the process, and is a solidification microstructure. This typical cast structure with porosity presence consists of three zones: the chill zone, the columnar zone and the equiaxed zone. Figure 5 shows these three zones in the fusion weld.

In practice, most castings solidify with a dendritic structure. The tendency for dendrites to grow in certain crystallographic directions affects the grain structure of castings. When liquid is poured into a mould, initial contact with the cold mould walls usually results in nucleation of a large number of small crystalls. This forms the so-called chill zone. Solidification occurs from each of these small crystalls, with the dendrites oriented in the corresponding easy growth directions.
Growth occurs more rapidly from crystals which have an easy growth direction parallel to the heat flow direction i.e. normal to the mould wall.
Less favourably-oriented crystals grow more slowly and tend to get pinched off by the more rapid growth of their neighbours.
In this way, the chill zone gives way to the columnar zone, consisting of grains elongated along the heat flow direction, which is close to one of their easy growth directions.
The grains in the columnar zone have different orientations from each other, because they are differently oriented in the plane normal to the heat direction.

The columnar zone may extend to the central plane of the casting. However, it often becomes possible for solids fragments (detached from growing dendrites by connection, or sedimentating from the free surface) to survive ahead of the advancing columnar grains. Such grain multiplication process can give rise to a central equiaxed zone, composed of randomly-oriented crystals.

The heat-affected zone (b), on the other hand, represents those regions in the close proximity of the weld, where the heat input during welding changes the microstructure of base metal without melting. It results in a coarse-grain microstructure.

The base metal (a) is the parent metal.

Figure 6 shows the macrostructure of the Friction stir processed zone and Figure 7 illustrates details of the variation of the microstructure corresponding to the regimes indicated by d-f in figure 6. The microstructure of the processed zone is formally divided into four areas: base metal, heat affected zone (HAZ), thermo-mechanically affected zone (TMAZ) and the nugget zone.
As shown in figure 6, from the base material to the weld centre, the crystal grains diminish gradually.

Figure 6. Macrostructure of the FSP zone.

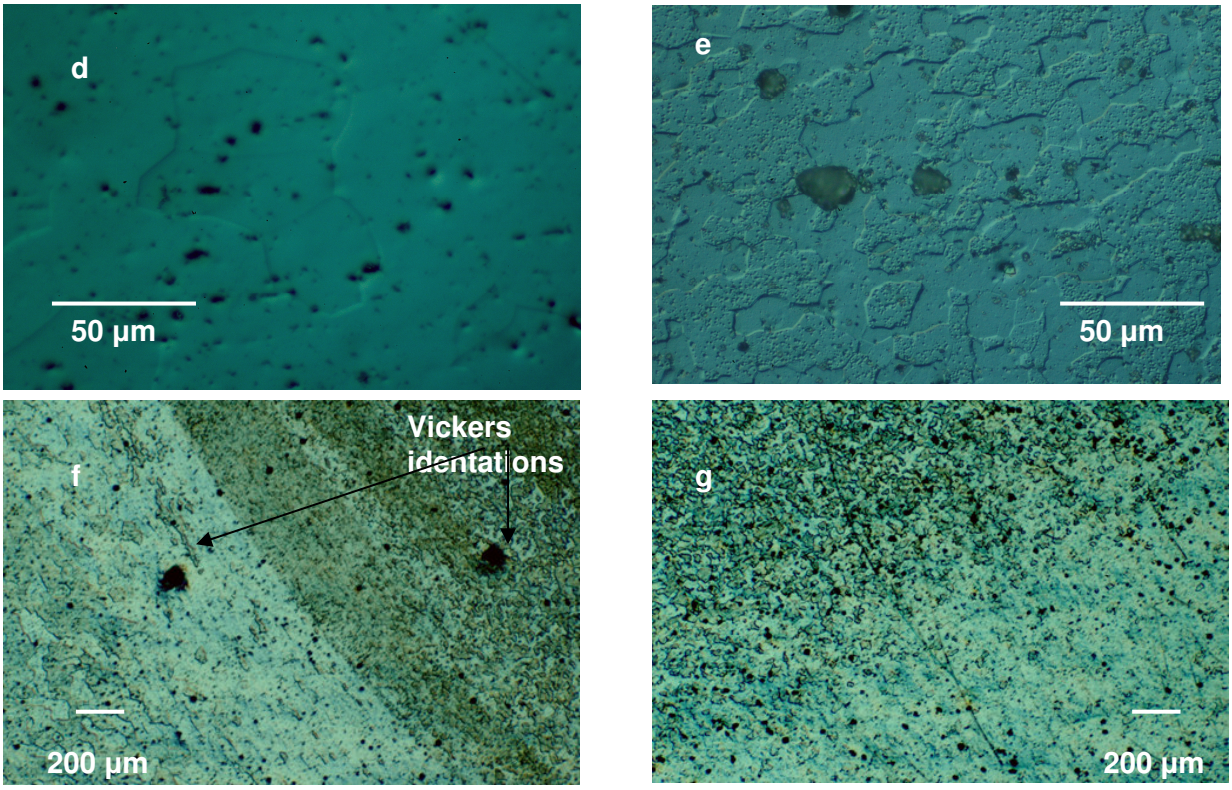

Figure 7. Microstructure variation of the processed zone: d) base metal, e) nugget, f) advancing side and g) retreating side.

The base material texture is an equiaxed grain structure with approximately 45 μm of crystal grain size.

The TMAZ microstructure consists of bent elongated grains near the nugget shown in the micrograph (f) and (g), and divided into the retreating side (RS) (Figure 3g) and the advancing side (AS) (Figure 3f) depending on different microstructures. Although both the advancing side and the retreating side have a boundary with the processed zone, the boundary in the advancing side is clearer than that in the retreating side. This phenomena is due to the different material flow in both sides.

The HAZ microstructure consists in heated affected base material grains.

The nugget is composed of fine-equiaxed recrystallized grains, which are formed under the high temperature and high rate of deformation of the process. The size of the crystal grain is about 15 μm.

Friction Stir Processing in the fusion welds lead to sound grain-refined processed zone without voids, cracks or distortion.

Hardness profiles

Hardness profile of the fusion weld is shown in figure 8.

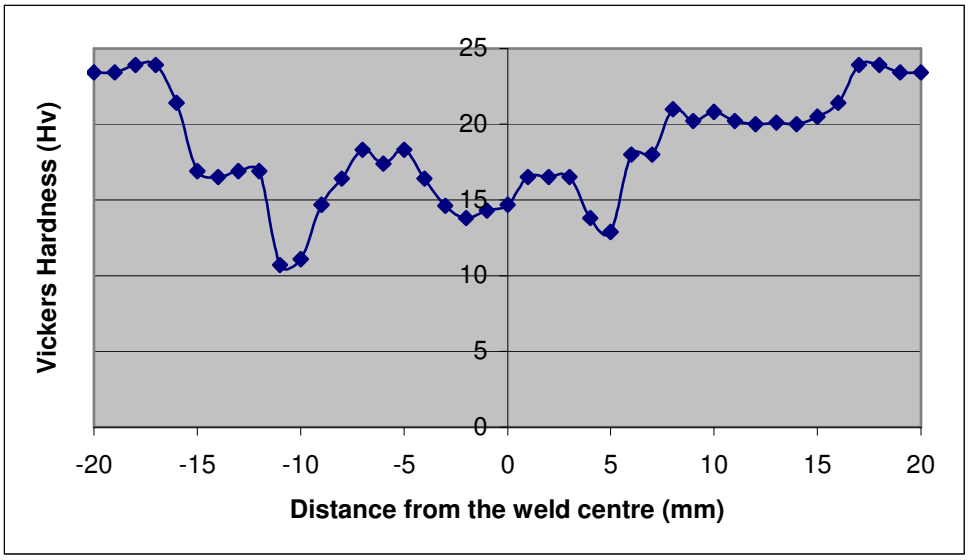

Figure 8. Hardness profile of the fusion weld toes.

As mentioned before, the fusion zone consists of as-cast coarse microstructure and coarse equiaxed grains occupy the heated-affected zone. These coarse microstructures lead to a hardness reduction in the fusion welds. Also the presence of porosity has a sound effect on this hardness reduction. Minimum hardness value of 11 HV is located at the transition region between the weld zone and the base material.

Hardness profile of the processed zone is presented in figure 9.

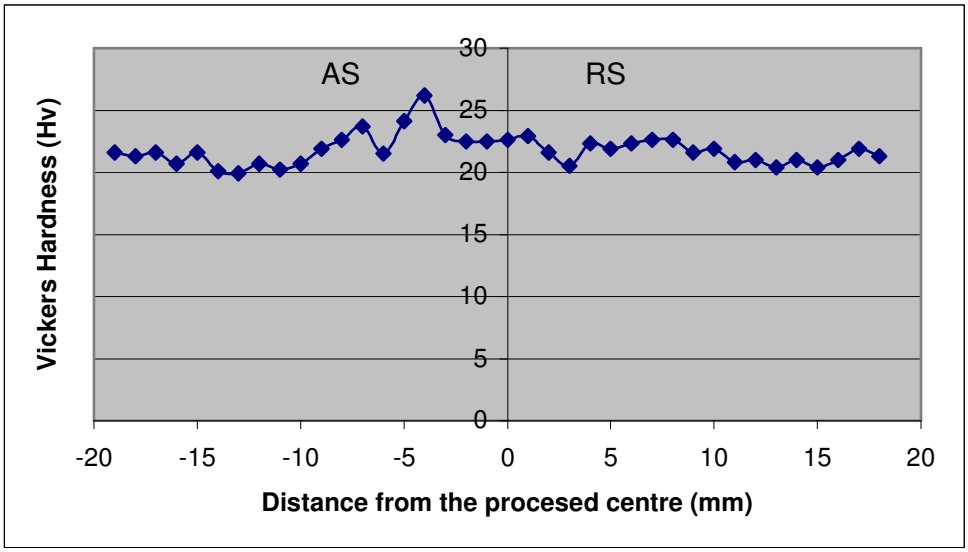

Figure 9. Hardness Profile of the processed zone.

A combination of grain refinement and porosity healing has lead an improvement in the mechanical properties of the fusion welds close to those in the base metal (~23Hv).

11.4 Conclusions

The TIG and FSP processes have been applied to Al 1050.

The TIG produced as-cast coarse microstructure and coarse equiaxed grain structure at the fusion zone and the heated affected zone respectively, which led to the hardness reduction to ~11HV in the TIG welds.

The subsequent FSP on the TIG welds obtained a fine grain microstructure with a cell size of ~12 μm and no porosity. This microstructure led to a high hardness close to the hardness base material.

From the present work, the following conclusion may be drawn. A variation of Friction Stir Welding (FSW), Friction Stir Processing (FSP), is viable to modify selected regions of materials to enhance specific properties while eliminating fusion welding defects such as porosity, cracking, and high tensile residual stresses caused by the solidification of the molten weld pool.

12. MICROSTRUCTURE IMPROVEMENT OF Al 1050-O

12.1 Introduction

On the bases of FSW, Friction Stir Processing (FSP) has emerged as a microstructure modifying technique resulting in a sound improvement on mechanical properties.

FSP was performed in Al 1050-O plates at a constant tool rotation rate and different tool traverse speeds ranging from 60 mm/min to 360 mm/min. The influence of the tool traverse speed on the microstructure and mechanical properties is discussed.

FSP leads to microstructures consisting of very fine grains with different densities of dislocations and various degree of recovery. Mechanical properties improvement such as hardness, depends on both how fine the gains are and how large the number of grains with high dislocations density and low degree of recovery is.

It is well-known that the hardness of 1050 aluminium alloy is primarily dependent on the grain size and the dislocation density.

In the present study, according to the recrystallization theory [24] presented on the paragraph “Recrystallization” from the present work, the contribution of the grain size hardening and the strain hardening to hardness is presented.

.

12.2 Experimental Procedures

The base material used in this study was Al 1050-O. As reported in the Alloys Studied paragraph, the alloy was presented in the annealed condition (1h-570℃) with a chemical composition of Al-0.25Si-0.4Fe-0.05Cu-0.05Mg-0.05Mn-0.07Zn-0.02Ti (all compositions are in wt.%). The average grain size was about 45 μm and the hardness value was approximately 21 HV. A rectangular plate having dimensions of 200 x 80 x 6 mm was prepared from the sheet of starting material. FSP using a tool with large diameter shoulder and a customized pin with a shorter length was performed. Diameter shoulder was 20 mm, diameter pin was 10 mm and pin length was 1 mm. Figure 1 shows the tool used.

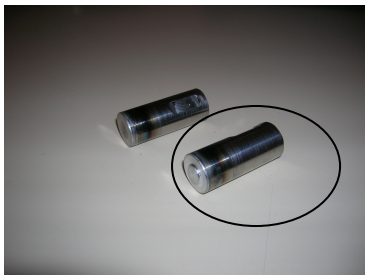

Figure 1. Tool used

The tool was rotated at a constant rotation rate of 500 rpm and advanced along the length direction of the workpiece at traverse speeds ranging from 60 to 360 mm/min. The processing parameters used in this study are summarized in table 1.

w (rpm)	v (mm/min)
500	60
500	120
500	180
500	240
500	300
500	360

Table 1. Processing parameters: tool rotation rate, w and tool traverse speed, v.

These conditions were used to make single stir passes with lengths of about 200 mm. Figure 2 presents a cross section perpendicular to the processed zone at 240 mm/min.

Figure 2. Cross section perpendicular to the processed zone at 240 mm/min.

Following the processes, Vickers hardness profiles were measured on the cross-section presented above. The microhardness measurements were made on metallographically prepared specimens. The specimens were cut in a rectangular shape having dimensions of 40 x 12 x 6 mm. Afterwards they were grinded using silicon carbide paper (220, 320, 500 and 1000) and polished with 6 μm diamond DP-suspension. Electropolishing was also applied. The indentations were made under a 50 g load extending from the processed zone into the base metal.

Grain structures in the processed zones were observed by optical microscopy under polarized light. The samples for optical microscopy where etched using HF 0.5% during at least 10 min.

12.3 Results

Temperature

Temperature profiles couldn't be measured experimentally. Though, in order to determine maximum temperatures reached within the friction stir zones processed at different tool traverse speeds, François model was used [19]. Based on Schmidt theory, presented on "temperature distribution and heat generation" paragraph from the present work, the model served to plot the following temperature profile (Figure 3):

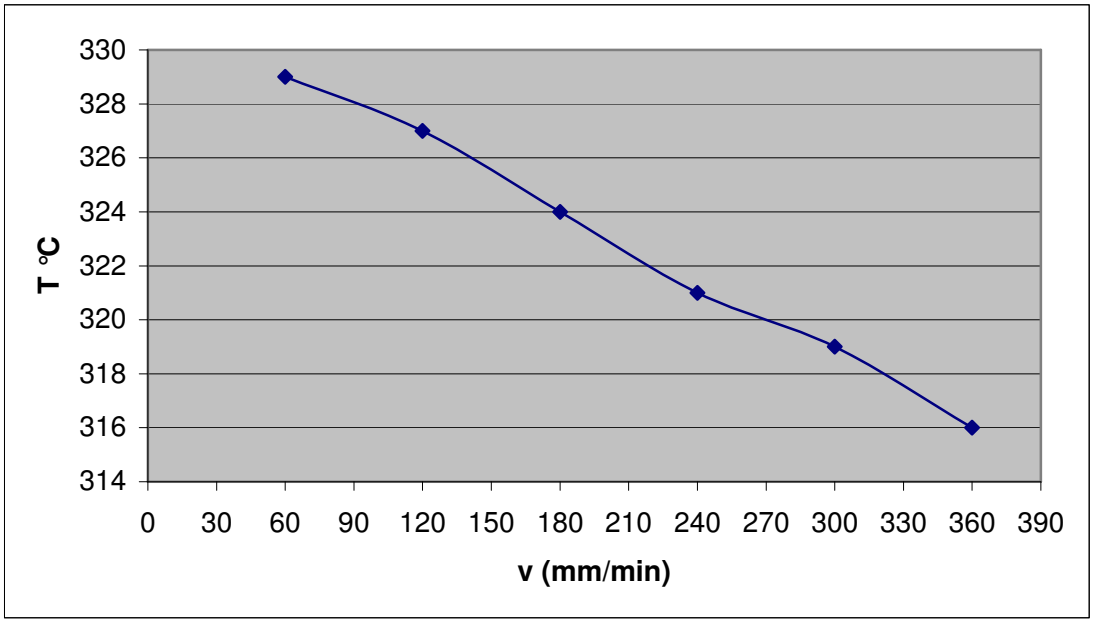

Figure 3. Temperature profile within the FSP zone.

Higher tool traverse speeds lead to lower heat generation. The maximum temperature linearly decreased from about 329 to 316°C with increase in tool traverse speed from 60 to 360 mm/min. Anyway, it couldn't be considered a significant change.
Since each maximum temperature was less than the melting point of the workpiece (650°C), it could be demonstrated that FSP experiments were carried out in the solid state.

Microstructure

Figure 4 shows the macrostructure of the Friction stir processed zone at 500 rpm rotation rate and 240 mm/min traverse speed. Similar macrostructures were obtained for the tool traverse speeds of 60, 120, 180, 300 and 360 mm/min. The microstructure of the processed zone is formally divided into four areas: base metal, heat affected zone (HAZ), thermo-mechanically affected zone (TMAZ) and the nugget zone. However, the present study was focused in the comparison between the base metal (a) and the nugget zone (b) microstructure.

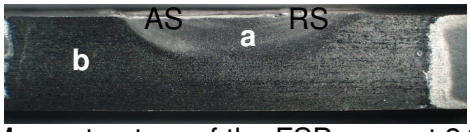

Figure 4. Macrostructure of the FSP zone at 240 mm/min

Figure 5 shows the optical micrographs of the base metal and the nugget zone of the friction stir processed samples at traverse speeds ranging from 60 to 360 mm/min.

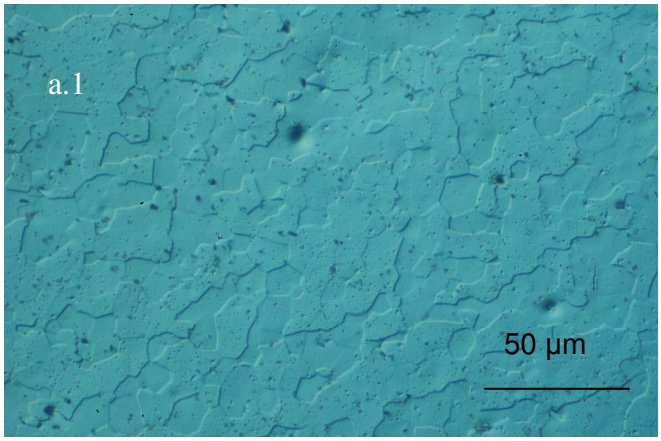

FSP 60 mm/min

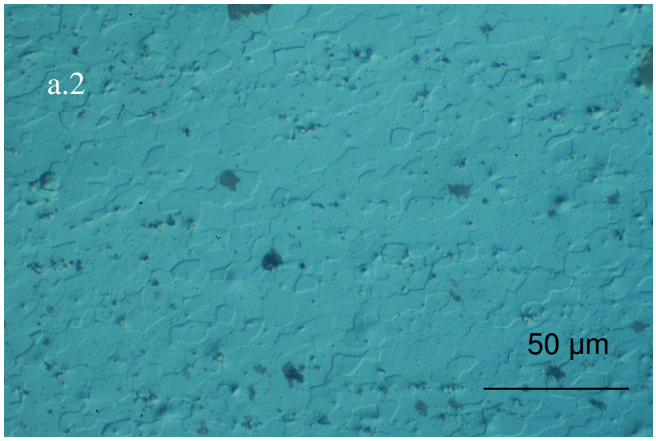

FSP 120 mm/min

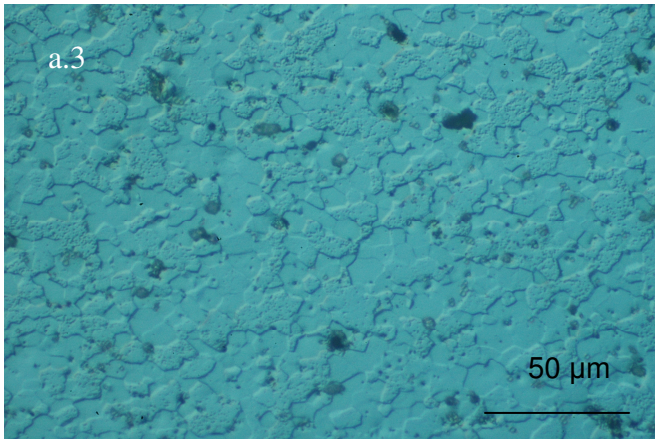

FSP 180 mm/min

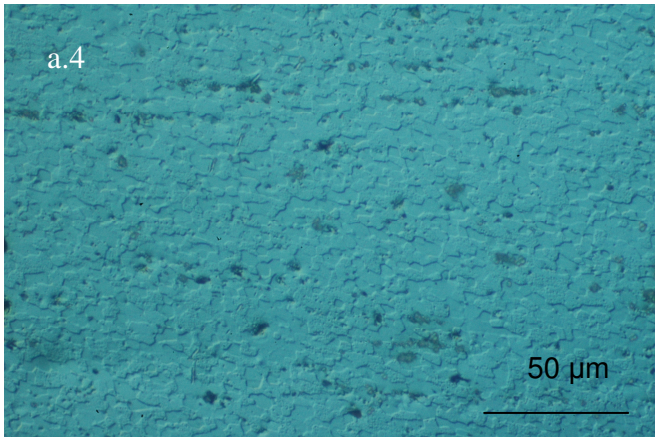

FSP 240 mm/min

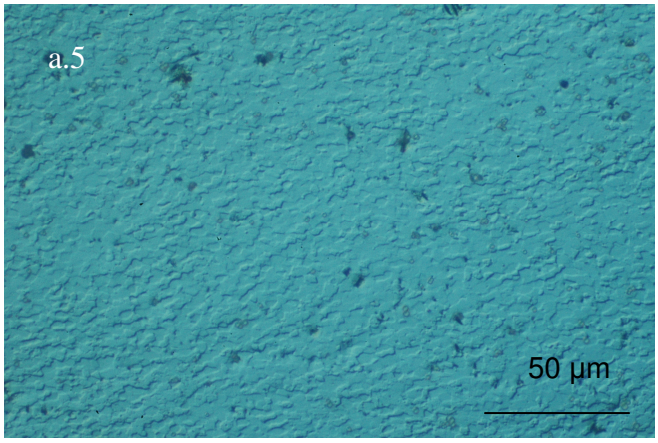

FSP 300 mm/min

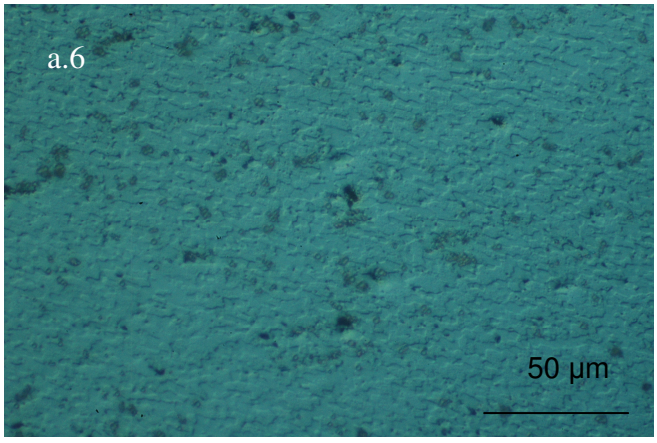

FSP 360 mm/min

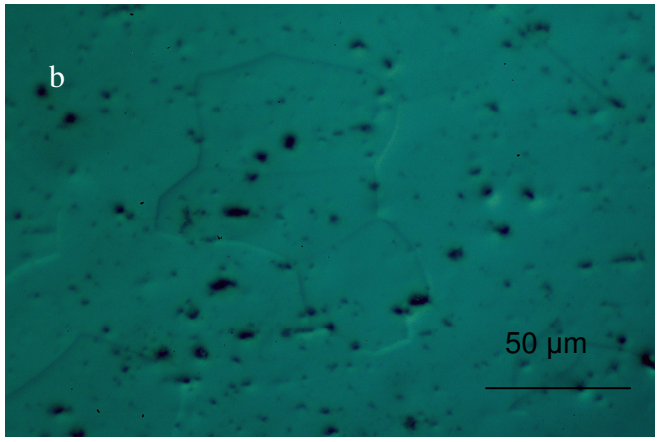

Base metal

Figure 5. Opical micrographs: a.1-a.6) nugget zones and b) base metal.

Comparing the base metal (b) with the friction stir processed zones (a.1, a.2, a.3, a.4, a.5 and a.6) a grain refinement in the nugget is clearly obtained. In order to quantify this grain refinement the grain size was calculated.

The base material texture was an equiaxed grain structure with approximately 45 μm of crystal grain size.

The nugget was composed of fine-equiaxed recrystallized grains, which were formed under the high temperature and high rate of deformation of the process. The size of the crystal grain ranged from ~11 μm for the minimum traverse speed (60 mm/min) to ~3 μm for the maximum traverse speed (360 mm/min).
In table 2 grain size values are collected.

		D (μm)
Base Metal, b		44,19
Nugget	v (mm/min)	
a.1	60	11,18
a.2	120	9,62
a.3	180	5,97
a.4	240	3,62
a.5	300	3,29
a.6	360	3,1

Table 2. Grain size values of base metal and FSP zones at different tool traverse speed.

From the data above it can be concluded that grain size decreased with increasing the tool traverse speed. The smaller grain size the bigger traverse speed. At 360 mm/min traverse speed, a grain size of ~3 μm was obtained. The grain size had decreased a 93%.

Unfortunately, TEM observations were not performed and dislocation densities could not be quantified. Generally, it was believed that the bigger tool traverse speed the bigger dislocation density. Thus, friction stir processed zones (a.1, a.2, a.3, a.4, a.5 and a.6) were supposed to have different dislocations densities. On the other hand, base metal in the annealed condition was assumed to have a low density of dislocations.

Due to an increase in traverse speed, comparing to the base metal microstructure, a decrease in grain size was obtained and an increase in dislocation densities was expected.

Hardness profiles

Figure 6 shows the Vickers microhardness distribution on the cross-section perpendicular to the tool traverse direction of the friction stir processed zones a.1, a.2, a.3, a.4, a.5 and a.6.

Microhardness values for the specimens processed at 120, 180, 240, 300 and 360 mm/min are higher in the friction stir processed zones than in the base metal. However, for the specimen processed at 60 mm/min a slightly difference is presented.

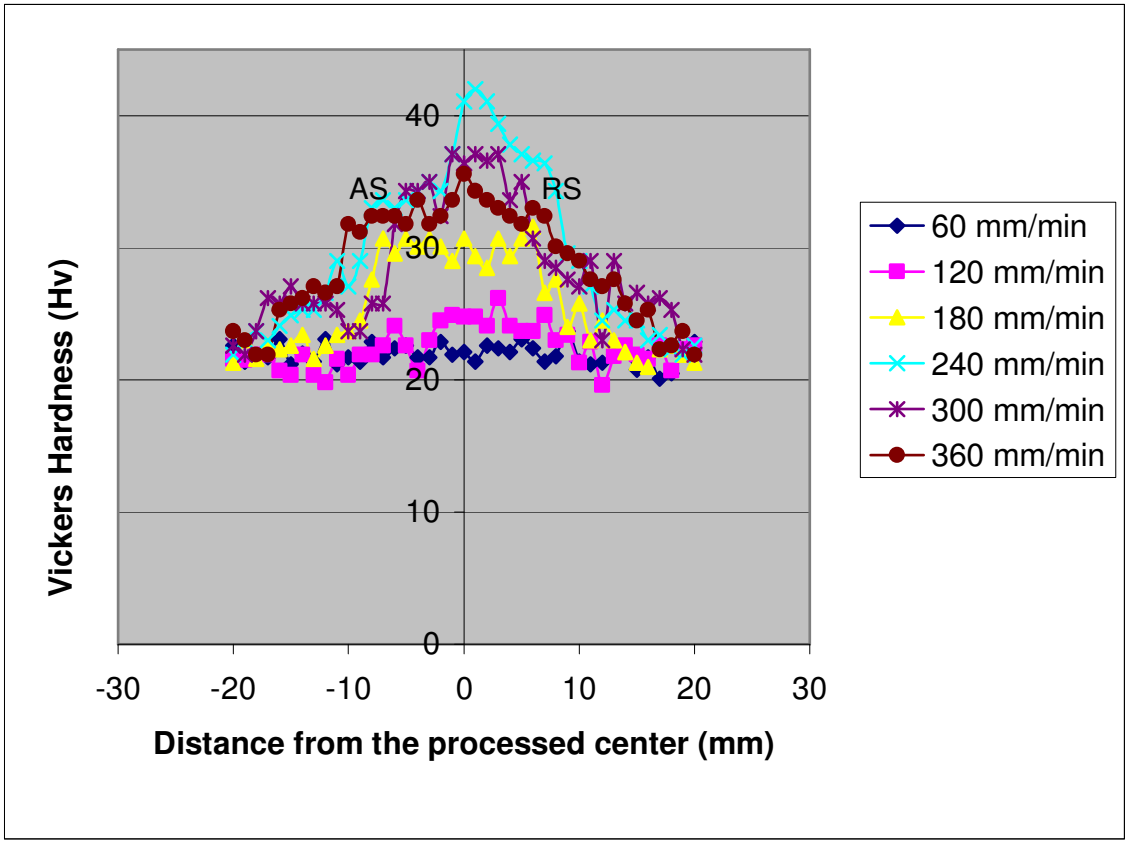

Figure 6. Microhardness values for the specimens processed at different tool traverse speeds.

When performing FSP at 60 mm/min traverse speed, no significant increase in hardness is observed. Maximum hardness value (23,7 Hv) is closed to the base metal hardness value (21 Hv).

Doubling the tool traverse speed to 120 mm/min, a slightly increase in hardness is obtained. Maximum hardness value is 26,2 Hv.

When processing at a tool traverse speed of 180 mm/min, a significant increase in hardness with a maximum hardness value of 31,6 Hv is presented.

For the specimen processed at 240 mm/min, the highest increase in hardness is obtained. 42 Hv is the highest hardness value achieved in friction stir processing Al 1050-O.

If processing is carried out at 300 mm/min, a sound increase in hardness is also presented. However, the maximum hardness value (37,1 Hv) is smaller than the one obtained at 240 mm/min traverse speed.

When traverse speed is increased to 360 mm/min, an increase on hardness is still obtained. Although, the maximum hardness value (35,6) is lower than the previous reached.

Figure 7 represents the maximum hardness values obtained at the different processing tool traverse speeds.

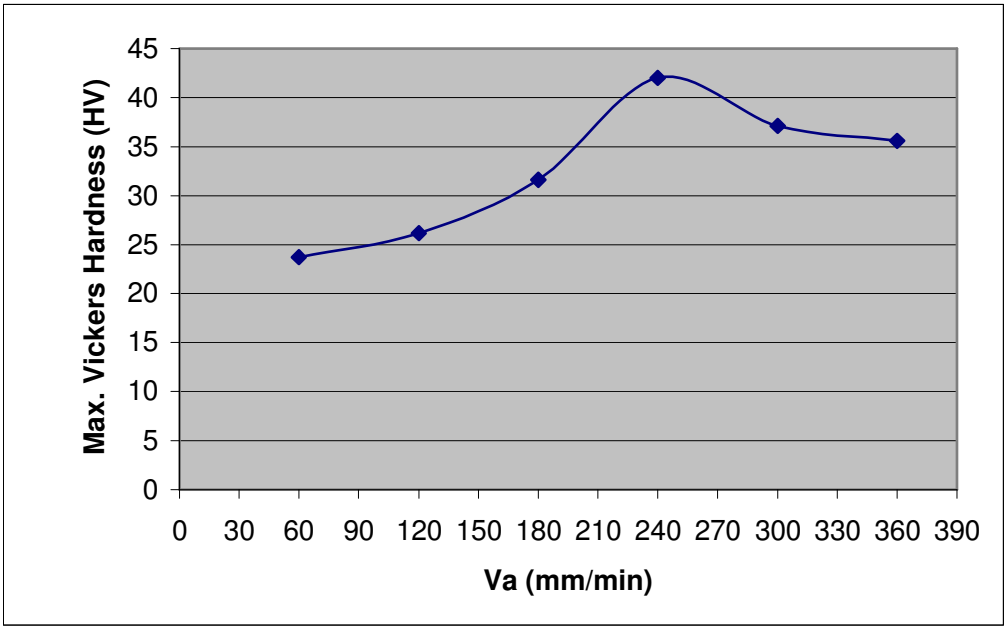

Figure 7. Maximum hardness values at different tool traverse speeds.

Comparing to the base metal, an increase in tool traverse speed lead to a significantly increase in hardness. Hardness increase value (ΔH) was calculated by the following way:

$\Delta H = H_{max\ i} - H_o$

where H_o was the base metal hardness value (21 Hv) and $H_{max\ i}$ were the maximum hardness values obtained at different tool traverse speeds i (60, 120, 180, 240, 300 and 360 mm/min).

Exact values and percentage values are presented in table 3:

	ΔH (Hv)	ΔH %
v (mm/min)		
60	2,7	12,86
120	5,2	24,76
180	10,6	50,48
240	21	100,00
300	16,1	76,67
360	14,6	69,52

Table 3. Increase in hardness (exact and percentage values).

12.5 Discussion

The influence of the tool traverse speed on the microstructure and mechanical properties such as hardness will be discussed.

Influence of the tool traverse speed on the microstructure

Generally, higher tool traverse speeds leads to lower heat generation and higher degree of deformation.
Low heat generation and high degree of deformation results in a sound grain refinement and a high dislocation density.

From the temperature profile obtained in figure 3, an increase in tool traverse speed leads to a decrease in heat generation. Such decrease prevents grain growth. Therefore, smaller grain size is expected.
In addition, low heat generation decreases diffusion. Thus, dislocation motion is prevented. Therefore, dynamic recovery is minimized and high dislocations density is expected.

Since Tem observations were not performed, strain plays an important role in both grain size refinement and dislocation density. In general, recrystallized grain size decreases with increase in strain. Furthermore, strain increases with increase in tool traverse speed. Tool traverse speed moves the stirred material from the front to the back of the pin, therefore higher tool traverse speed leads to bigger degree of deformation.

In summary, the grain size refinement and high dislocations density obtained increasing tool traverse speed from 60 mm/min to 360 mm/min is supposed to be caused by both, a decrease in temperature and an increase in strain.

Influence of the tool traverse speed on hardness

It is well-known that the hardness of 1050 aluminium alloy is primarily dependent on the grain size and the dislocation density.

From the results, it was concluded that hardness increased when increasing tool traverse speed. Table 3 presents hardness increase exact values and percentage values obtained.

To quantify the contribution of the grain size refinement in hardness increase Hall-Petch relationship was used:

$$H_v = H_o + K_H d^{-1/2}$$

where H_o and K_H are the appropriate constants associated with the hardness measurements, and d is the average grain diameter.

For Al 1050-O, K_H is about 9 Hv $\mu m^{1/2}$ [15]. So the relationship can be written as follows:

$$H_v - H_o = 9d^{-1/2}$$

For each grain size obtained in the friction stir processed zones performed at different tool traverse speeds, the grain size hardening is calculated. Table 4 shows the grain size hardening.

	d (um)	Grain size hardening (Hv)
v (mm/min)		Hall Petch
60	11,18	2,69
120	9,62	2,90
180	5,97	3,68
240	3,62	4,73
300	3,29	4,96
360	3,1	5,11

Table 4. Grain size hardness due to the Hall-Petch relatioship.

Increasing tool traverse speed increases grain size hardening. However grain size hardening doesn't explain entirely the hardness increase presented in table 3.
Table 5 collects the contribution of grain size hardening to the hardness increase. Exact values and percentage values are presented.

	ΔH (Hv)	Grain size Hardening (Hv)	ΔH %	Grain size Hardening %
v (mm/min)		Hall Petch		
60	2,7	2,69	12,86	12,82
120	5,2	2,90	24,76	13,82
180	10,6	3,68	50,48	17,53
240	21	4,73	100,00	22,50
300	16,1	4,96	76,67	23,61
360	14,6	5,11	69,52	24,34

Table 5. Contribution of grain size hardening to the hardness increase.

Only when processing at 60 mm/min tool traverse speed, the grain size hardening contributes almost totally to the hardness.

At 120 mm/min tool traverse speed, the grain size hardening has a significant effect to the hardness.

For the rest of tool traverse processing parameters (180, 240, 300 and 360 mm/min), the grain size hardening contributes less to the hardness. In those conditions, hardness of the friction stir zones is more dependent on the dislocation density than the grain size.

Strain hardening explains the increase in hardness that grain size hardening can not.

Table 6 shows the contribution of strain hardening to the hardness increase. Exact values and percentage values are presented.

	ΔH (Hv)	Strain Hardening	ΔH %	Strain Hardening %
v (mm/min)				
60	2,7	0,01	12,86	0,04
120	2,6	2,30	24,76	10,95
180	10,6	6,92	50,48	32,94
240	21	16,27	100,00	77,50
300	16,1	11,14	76,67	53,06
360	14,6	9,49	69,52	45,19

Table 6. Contribution of strain hardening to the hardness increase

Strain hardening is the major factor capable to explain the hardness increase when processing at 180, 240, 300 and 360.

Increasing tool traverse speed from 60 mm/min to 240 mm/min, increases strain hardening.

When processing at 240 mm/min tool traverse speed, an optimal strain hardening is presented.

For tool traverse speeds higher than 240 mm/min (300 and 360 mm/min), the strain hardening decreases slightly.

In conclusion, hardness increase is dependent on two factors: grain size hardening and strain hardening. The contribution of each to such increase, changes when varying tool traverse speed.

Table 7 collects the contribution of grain size hardening and strain hardening to the hardness increase, in percentage.

	ΔH %	Grain size hardening %	Strain Hardening %
v (mm/min)			
60	12,86	12,82	0,04
120	24,76	13,81	10,95
180	50,48	17,54	32,94
240	100,00	22,50	77,50
300	76,67	23,61	53,06
360	69,52	24,34	45,19

Table 7. Contribution of grain size hardening and strain hardening to the hardness increase (%).

When performing FSP at 60 mm/min, hardness increased to about 12.86%. 12.82% increase corresponds to the grain size hardening and only 0.04% increase to the strain hardening.

Doubling the tool traverse speed to 120 mm/min, 24.76% increase in hardness is obtained. 13.81% increase, is induced by the grain size hardening and 10.95% increase by the strain hardening.

These results suggest that the hardness of the friction stir zones processed at 60 mm/min and 120 mm/min are more dependent on the grain size than the dislocation density.

When processing at a tool traverse speed of 180 mm/min a significant increase in hardness of 50.48% is presented. 32.94% increase, correspond to the strain hardening and 17.54% increase to the grain size hardening.

For the specimen processed at 240 mm/min the highest increase in hardness is obtained. The hardness is doubled. From this 100% increase, 77.5% increase, is generated by the strain hardening and 22.5% increase by the grain size hardening.

If processing is carried out at 300 mm/min, hardness increases to about 76.67%. 53.06% increase, correspond to the strain hardening and 23.61% increase to grain size hardening.

When traverse speed is increased to 360 mm/min, a lower increase on hardness (69.52%) is achieved. 45.19% increase, is caused by the strain hardening and 24.33% increase by the grain size hardening.

From the discussion above, it can be concluded that the hardness of the friction stir zones processed at 180, 240, 300 and 360 mm/min is more dependent on the dislocation density than the grain size.

According to the recrystallization theory [24] presented on the paragraph “Recrystallization” from the present work, the increase in hardness will be explained. In

addition, the contribution of the grain size hardening and the strain hardening in such increase will be discussed.

Due to non-uniform plastic deformation introduced in recystallized grains, it is believed that the final microstucture in FSP consists of some grains that are result of growth of initial recrystallized grains while others are formed from subgrains via continuous dynamic recrystallization.

The following schema illustrates the two possible recystallization models.

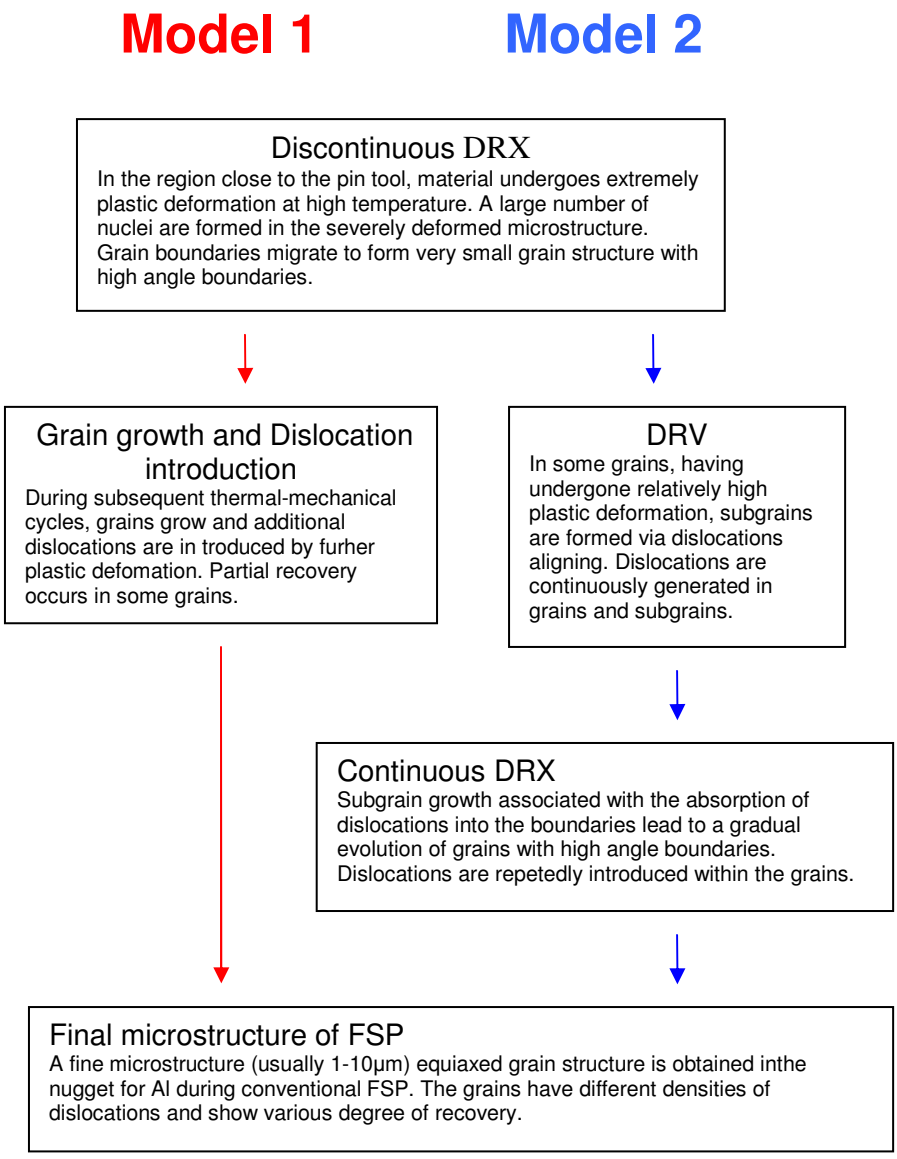

Figure 8. Recrystallization models [24].

As the schema presents, microstructure evolution is the result of various mechanisms.

Model 1 includes discontinuous dynamic recrystallization, grain growth and dislocation introduction. Therefore, model 1 leads to a final equiaxed microstructure with a high density of dislocations.

Model 2 includes discontinuous dynamic recrystallization, dynamic recovery and continuous dynamic recrystallization. Thus, in model 2 low densities of dislocations are expected.

For friction stir processed zones where the hardness increase is more dependent on strain hardening, the number of the grains formed in model 1-recrystallization is expected to be higher than the ones formed in model 2. The percentage of the number of grains recrystallized in model 1 is supposed to be the contribution of the strain hardening to the hardness increase.

On the other hand, when the hardness increase is more dependent on grain size hardening, the number of the grains evolved according model 2 is expected to be higher than the ones evolved according to model 1. The percentage of the number of grains recrystallized in model 2 is supposed to be the contribution of the grain size hardening to the hardness increase.

Table 8 represents the percentage of the grains evolved according to model 1 and model 2 at different tool traverse speeds.

	% of recrystallized grains Model 1	% of recrystallized grains Model 2
v (mm/min)		
60	0,31	99,69
120	44,21	55,79
180	65,27	34,73
240	77,50	22,50
300	69,21	30,79
360	64,99	35,01

Table 8. Percentage of the grains developed according to model 1 and model 2.

When performing FSP at 60 mm/min, almost all the grains (99.69%) recrystallize according to model 2. Only 0.31% of the gains do it according to model 1. Therefore, dislocation presence is supposed to be almost inexistent. Thus, the hardness increase is more dependent on grain refinement than dislocations density.

Doubling the tool traverse speed to 120 mm/min, slightly more than half of the grains are formed in model 2-recystallization and the rest in model 1. This means that more or less grain refinement and dislocations density play the same role in the hardness increase.

The results above suggest that the hardness of the friction stir zones processed at 60 mm/min and 120 mm/min is more dependent on the grain size than the dislocation density. In order to this, model 2 results to be the main recystallization model.

When processing at a tool traverse speed of 180 mm/min, 65.27% of the grains undergoes a model 1-recrystallization and the remaining percentage a model 2 one.

For the specimen processed at 240 mm/min, the one with the highest increase in hardness, 77.5% of the grains recrystallize following model 1 and 22.5% of them following model 2. Thus, a sound dislocation density within the grains is expected to be presented.

If processing is carried out at 300 mm/min, 69.21% of the grains are developed according to model 1 and the rest according to model 2. Comparing to 240 mm/min tool

traverse speed, the number of grains evolved according to model 1 decreases. Thus, strain hardening contributes less to the hardness. Therefore lower hardness is noted.

When traverse speed is increased to 360 mm/min, 64.99% of the grains undergoes a model 1-recrystallization and 35.01% of them a model 2 one. Comparing to 240 mm/min and 300 mm/min tool traverse speeds, grain size hardening increases in influence. Furthermore, the number of grains recystallized in model 1 decreases. Thus, lower hardness is presented.

The discussion above, suggest that the hardness of the friction stir zones processed at 180, 240, 300 and 360 mm/min is more dependent on the dislocation density than the grain size. This means that the number of the grains formed according to model 1 is higher than the ones formed according to model 2. In order to this, model 1 resulted to be the main recystallization model.

At this stage the following remarks may be presented:

Higher tool traverse speeds leads to higher number of grains formed in model 1-recrystallization. Thus, the strain hardening becomes more important than grain size hardening in hardness increase. As a result, the increase in hardness goes higher and higher until the optimum is reached.

Processing at 240 mm/min tool traverse speed, involves the highest number of grains developed by model 1. Therefore, the highest strain hardening contribution to the hardness increase is presented. In order to this, the highest hardness is obtained.

For tool traverse speeds higher than the optimum, the number of grains recrystallized in model 1 decrease. Also, the influence of the strain hardening in the hardness increase becomes smaller. As a consequence, the result is a decrease in hardness.

Table 9 collects the information in table 7 and 8.

	ΔH %	Grain size hardening %	Strain Hardening %	% of recrystallized grains Model 1	% of recrystallized grains Model 2
v (mm/min)					
60	12,86	12,82	0,04	0,31	99,69
120	24,76	13,81	10,95	44,21	55,79
180	50,48	17,54	32,94	65,27	34,73
240	100	22,5	77,5	77,5	22,5
300	76,67	23,61	53,06	69,21	30,79
360	69,52	24,34	45,19	64,99	35,01

Table 9. Contribution percentage of grain size hardening and strain hardening to the hardness increase and percentage of the grains developed according to model 1 and model 2 .

The data collected in table 9 leads to the following discussion:

For friction stir zones processed at 60, 120, 180 and 240 mm/min, an increase in tool traverse speed leads to an increase in hardness.
The number of grains recrystallizated according to model 1 increases, and at the same time, the number of grains formed in model 2-recrystallization decreases. Therefore, the contribution of the strain hardening to the hardness becomes larger and more

important. Moreover, the contribution of the grain size hardening to the hardness gets also larger but less important. Thus, a high dislocation density is presented.

For friction stir zones processed at 300 and 360 mm/min, an increase in tool traverse speed leads to a decrease in hardness.
The number of grains developed according to model 1 decreases while the number of the ones evolved according to model 2 increases. Therefore, the contribution of the strain hardening to the hardness becomes smaller, and the contribution of the grain size hardening gets larger.
Although the contribution of the strain hardening to the hardness still remains more important, a lower dislocation density is presented.

The discussion above is schematically illustrated in figure 9.

a) For friction stir zones processed at 60, 120, 180 and 240 mm/min

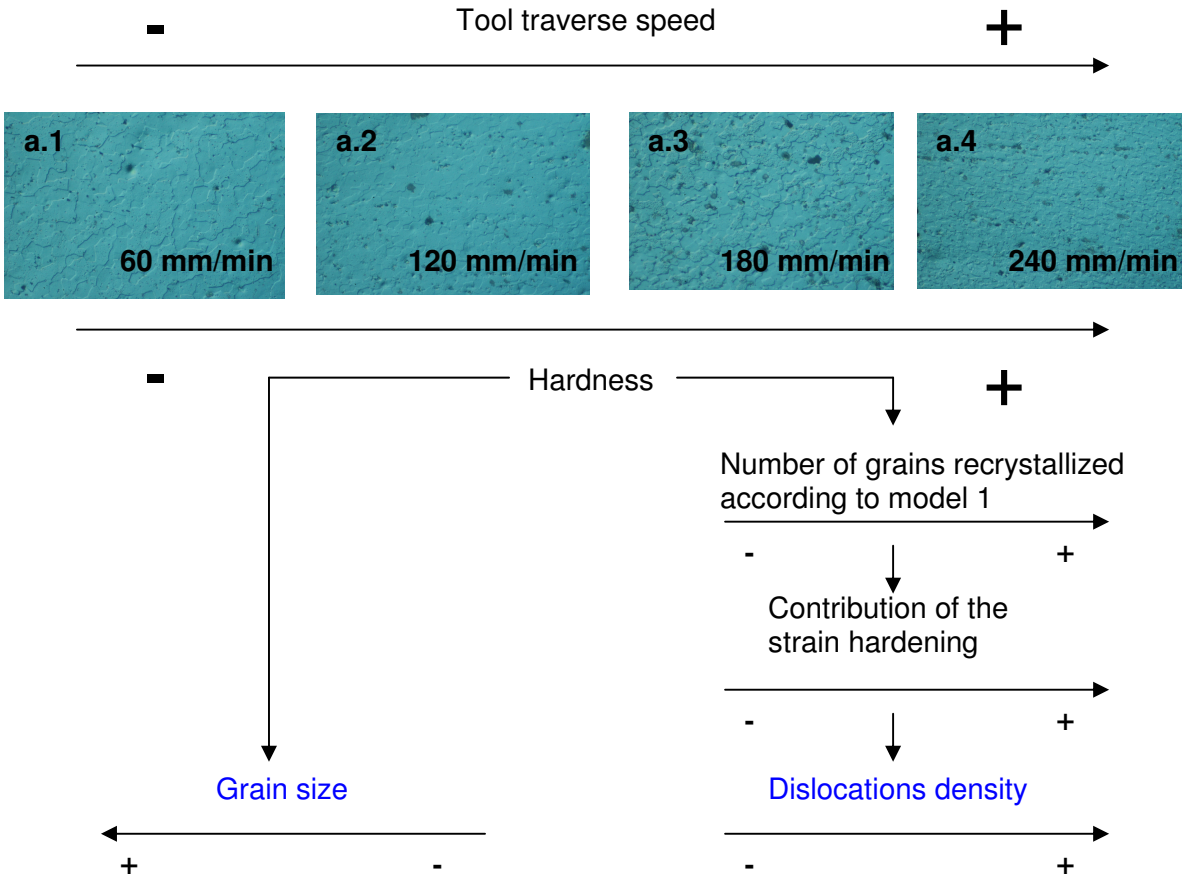

b) For friction stir zones processed at 300 and 360 mm/min.

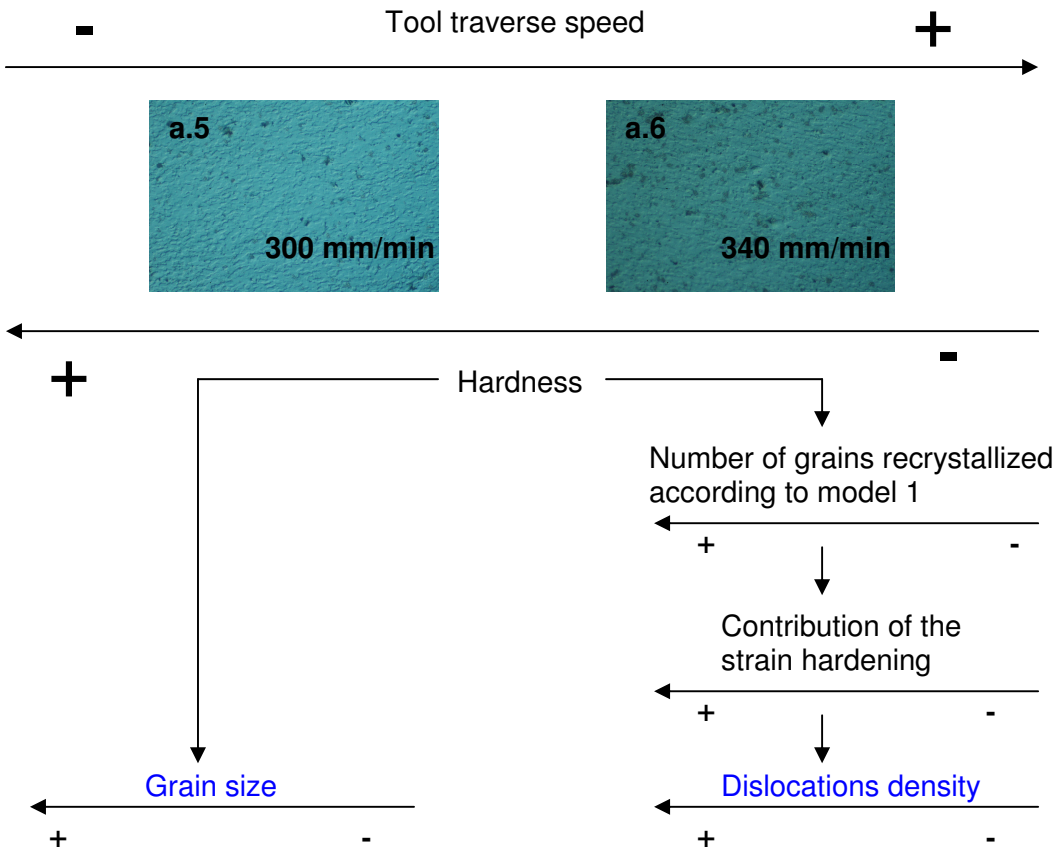

Figure 9. Effects on microstructure and mechanical properties increasing tool traverse speed: a) For friction stir zones processed at 60, 120, 180 and 240 mm/min and b) For friction stir zones processed at 300 and 360 mm/min.

Definitely, in order to probe the results presented schematically, further experimental work such as TEM observations is needed

12.6 Conclusions

1050-O aluminium alloy was processed through only a single pass of the FSP under various tool traverse speeds ranging from 60 mm/min to 360 mm/min. The influence of the tool traverse speed on the hardness of the friction stir-processed 1050 aluminium alloy was experimentally investigated. Also, the influence of the tool traverse speed on the temperature profile was obtained by modelling.

The following results were obtained:

-Generally, higher tool traverse speeds leads to lower heat generation and higher degree of deformation. Low heat generation and high degree of deformation result in a sound grain refinement and relatively high degree of dislocations density.

According to these general issues, in the present work:

-Higher tool traverse speeds lead to lower heat generation. The maximum temperature linearly decreased from about 329 to 316℃ with increase in tool traverse speed from 60 to 360 mm/min. Such decrease prevents grain growth. Therefore, smaller grain size was expected.

-Grain size decreased with increasing the tool traverse speed. The smaller grain size the bigger traverse speed. At 360 mm/min traverse speed, a grain size of ~3 μm was obtained. The grain size had decreased a 93%.

-Microhardness values for the specimens processed at 120, 180, 240, 300 and 360 mm/min were higher in the friction stir processed zones than in the base metal. Although, for the specimen processed at 60 mm/min a slightly difference was presented.

-It is well-known that the hardness of 1050 aluminium alloy is primarily dependent on the grain size (grain size hardening) and the dislocation density (strain hardening).

Using the recrystallization presented in the paragraph "Recrystallization" from the present work, the contribution of both, grain size hardening and strain hardening, to the increase in hardness was discussed.

-Higher tool traverse speeds lead to higher number of grains formed in model 1-recrystallization. Thus, the strain hardening became more important than the grain size hardening in hardness. As a result, the increase in hardness went higher and higher until the optimum was reached.

-Processing at 240 mm/min tool traverse speed involved the highest number of grains developed by model 1. Therefore, the highest strain hardening contribution to the hardness was presented. In order to this, the highest hardness (42Hv) was obtained.

-For tool traverse speeds higher than the optimum, the number of grains recrystallized in model 1 decreased. Moreover, the influence of the strain hardening in hardness became smaller. As a consequence, the result was a decrease in hardness.

Definitely, in order to probe the results presented above, further experimental work such as TEM observations is needed

13. REFERENCES

[1] W. M. Thomas et al., “Friction Stir Welding”, G. B. Patent Application Nº. 9125978.8, Dec. 1991; US Patent Nº. 5460317, Oct. 1995.
[2] R.S. Mishra, Z. Y. Ma. Friction Stir welding and processing. Material Science and engineering R 50 (2005) 1-78
[3] M.W. Mahoney and S.P. Lynch. Friction Stir Processing.
http://www.darpa.mil/dso/thrust/matdev/fsp/pdfs/fspsem_a1.pdf
[4] www.darpa.mil/dso/thrust/matdev/fsp/about.html
[5] www.msm.cam.ac.uk/phase-trans/2003/FSW/aaa.html
[6] C.G. Rhodes, M.W. Mahoney, W.H. Bingel, M. Calabrese. Fine-grain evolution in friction-stir processed 7050 aluminium. Scripta Materialia 48 (2003) 1451-1455
[7] R.S. Mishra, M.W. Mahoney, S.X. Mc Fadden, N.A. Mara and A.K. Mukherjee. High Strain Rate Superplasticity in a Friction Stir Processed 7075 Al Alloy. Scripta Materialia 42 (2003) 163-168
[8] Z.Y. Ma, R.S. Mishra, M.W. Mahoney. Superplasticity in cast A365 induced via friction Stir Processing. Scripta Materialia 50 (2004) 931-935
[9] R.S. Mishra, Z.Y. Ma, I. Charit. Friction Stir Processing : a novel technique for fabrication of surface composite. Material Science and engineering A 341 (2003) 307-310
[10] M.L Santella, T. Engstron, D. Storjohann, T-Y. Pan. Effects of friction stir processing on mechanical properties of the cast aluminium alloys A319 and A356. Scripta Materialia 53 (2005) 201-206
[11] Z.Y. Ma, S. R. Sharma, R.S. Mishra, M.W. Mahoney. Microstructural modification of cast aluminium alloys via friction stir processing. Materials Science F 426-432 (2003) 998
[12] K. Oh-ishi, A.M. cuevas, D.L. Swisher and T. R. McNelley. The influence of Friction Stir Processing on Microstructure and properties of Cast Nickel Aluminium Bronze Material. Metallurgical and Materials Transactions A: Physical Metallurgy and Materials Science 36 (2005) 1575-1585
[13] M.W. Mahoney, W. H. Bingel and R.S. Mishra. Microstructural Modification and Resultant Properties of Friction Stir Processed Cast NiAl Bronze. Metallurgical and Materials Transactions A: Physical Metallurgy and Materials Science A 35 (2004) 2951-2961
[14] Y. S. Sato, Mitsunori Urata, Hiroyuki Kokawa, Keisuke Ikeda and Masatoshi Enomoto. Retention of fine grained microstructure of equal channel angular pressed aluminium alloy 1050 by friction stir welding. Scripta Materialia 45 (2001) 109-114
[15] Y. S. Sato, Mitsunori Urata, Hiroyuki Kokawa, Keisuke Ikeda. Hall-Petch relationship in friction stir welds of equal channel angular-pressed aluminium alloys. Material Science and engineering A 354 (2003) 298-305
[16] Y.J. Known, I. Shigematsu, N. Saito. Mechanical properties of fine-grained aluminium alloy produced by friction stir process. Scripta Material 49 (2003) 785-789
[17] N. Saito, T. Komaya et al. Grain refinement of 1050 aluminium alloy by friction stir processing. Journal of materials science letters 20 (2001) 1913–1915
[18] Y.J. Known, N. Sato, I. Shigematsu. Friction stir process a new refinement technique of ultrafined grained aluminium alloy. Journal of materials science letters 21 (2002) 1473–1476
[19] F. Gratecap, G. Racineux, A. Poitou. Influence of process parameters on friction stir welding conditions-Application to 6061 T6 Al alloy thin plates. Unpublished results.
[20] H. Schmidt, J. Hattel et al. An analytical model for the heat generation in friction stir welding. Modelling and Simulation in Materials Science and Engineering 12 (2004) 143-157
[21] F. J. Humphreys and M. Hartley. Recrystallization and Related Annealing Phenomena. Pergamon, ISBN 0 08 041884 8

[22] K. V. Jata and S. L. Semiatin. Continuous dynamic recrystallization during friction stir welding of high strength aluminium alloys. Materials Science and Engineering A 405 (2005) 277–286
[23] J. Q. Su, T. W. Nelson et al. Microstructural investigation of friction stir welded 7050-T651 aluminium. Acta Materialia 51 (2003) 713-729
[24] J. Q. Su, T. W. Nelson et al. Microstructure evolution during FSW/FSP of high strength aluminium alloys. Material Science and engineering A 405 (2005) 277-286